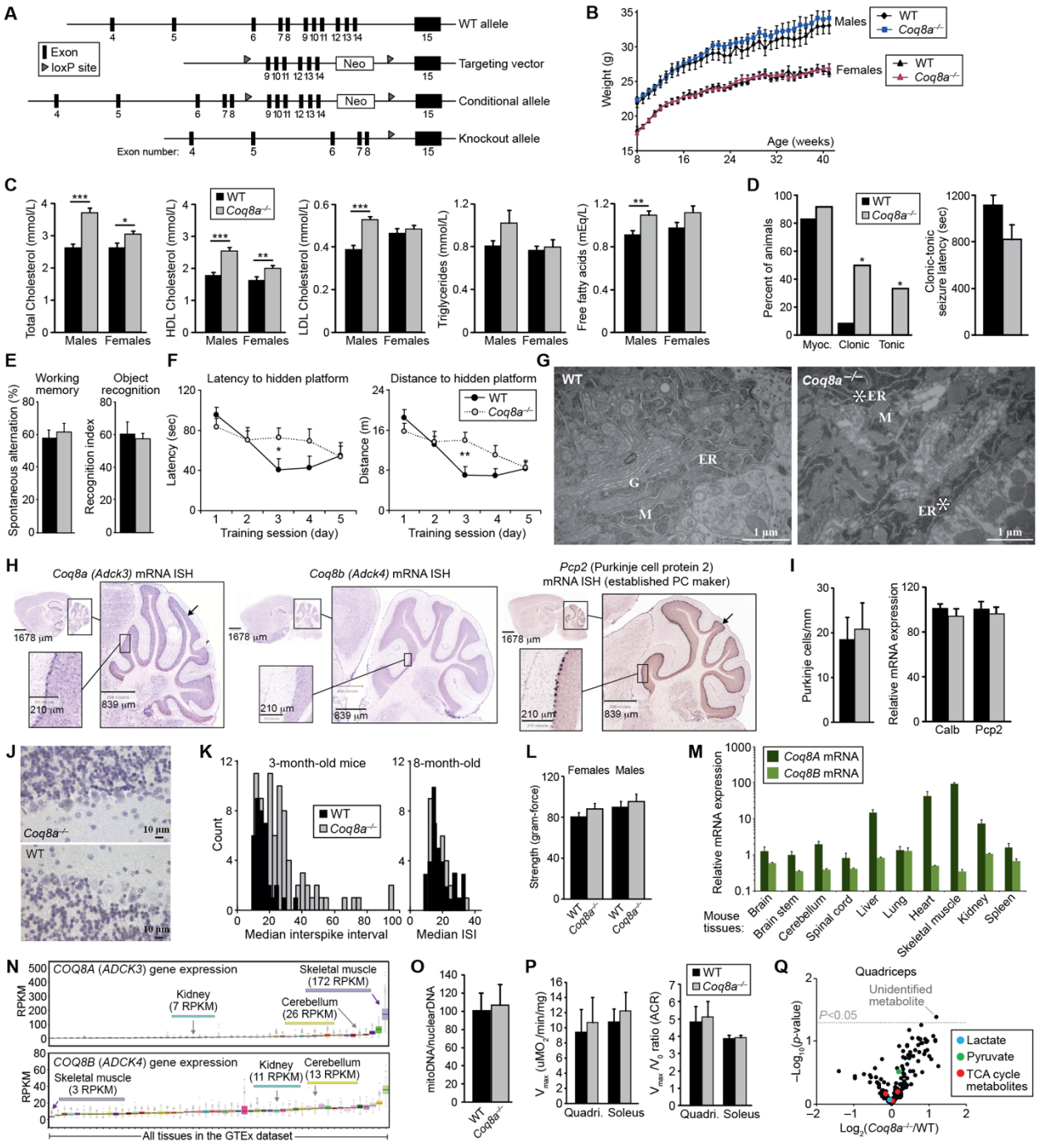

Figure S1, related to Figure 1. Generation and Characterization of *Coq8a*$^{-/-}$ Mice

(A) Scheme of constructs used to generate the *Coq8a*$^{-/-}$ mice.

(B) Body weight of WT and *Coq8a*$^{-/-}$ mice over time (mean ± SEM, n = 9).

(C) Blood lipid measurements in 25-week-old mice (mean ± SEM, n = 9).

(D) Susceptibility to epilepsy tested by PTZ injection in 6-month-old WT and *Coq8a*$^{-/-}$ mice. Left, percentage of mice that displayed myoclonic, clonic, or tonic crisis. Right, latency to clonic-tonic seizure (mean ± SEM, n = 12).

(E) Y-maze spontaneous alternation (left) and recognition memory (right) assessed in WT (black) and *Coq8a*$^{-/-}$ (gray) mice (5-month-old) (mean ± SEM, n = 12).

(F) Latency (left) and distance (right) to reach a hidden platform assessed by Morris water maze test in 5-month-old mice (mean ± SEM, n = 12).
(G) Representative electron microscopy images of WT and *Coq8a*$^{-/-}$ cerebella (30-week-old mice). G, Golgi apparatus; ER, endoplasmic reticulum; *dilated ER cisternae; scale bar, 1 μm.
(H) Allen Brain Atlas (mouse brain; http://mouse.brain-map.org) (Lein et al., 2007) in situ hybridization (ISH) images for *Coq8a*, *Coq8b*, or *Pcp2* mRNA. Arrows indicate a layer of distinct Purkinje cell bodies visible as puncta of ISH signal.
(I) Purkinje cell number in cerebellar H&E sections (left), and mRNA expression of cerebellar markers (*Calbindin* and *Pcp2*) (right) of WT (black) and *Coq8a*$^{-/-}$ (gray) mice (22-month-old) (mean ± SEM, n = 5).
(J) Representative TUNEL staining of cerebellar sections, 16-month-old mice. Scale bar 10 μm.
(K) Distribution of the median interspike intervals (ISI) of Purkinje cells recorded in acute cerebellar slices from 3-month-old (left) and 8-month-old (right) mice. Number of cells > 40.
(L) Strength of 10-week-old mice assessed by grip test (mean ± SEM, n = 8–12).
(M) Relative mRNA expression levels of *Coq8a* and *Coq8b* across various mouse tissues as quantified by RT-PCR (mean ± SEM, n = 3).
(N) mRNA expression data for *COQ8A* (*ADCK3*) and *COQ8B* (*ADCK4*) across human tissues as reported in the GTEx dataset (http://www.gtexportal.org) (Consortium, 2015). RPKM, reads per kilobase per million mapped reads.
(O) Mitochondrial content quantified as the ratio mitochondrial DNA/nuclear DNA by qRT-PCR of quadriceps muscle (18-month-old mice) (mean ± SEM, n = 7).
(P) Mitochondrial respiration (left, maximum O_2 consumption, V_{max}; right, V_{max}/V_0 ratio) of skeletal muscle fibers (10-month-old mice) (mean ± SD, n = 8).
(Q) Fold changes in mouse metabolite abundances ($\log_2$(*Coq8a*$^{-/-}$/WT), mean, n = 4) as quantified by GC-MS analysis.
For all panels: *P<0.05, **P<0.01, ***P<0.001.

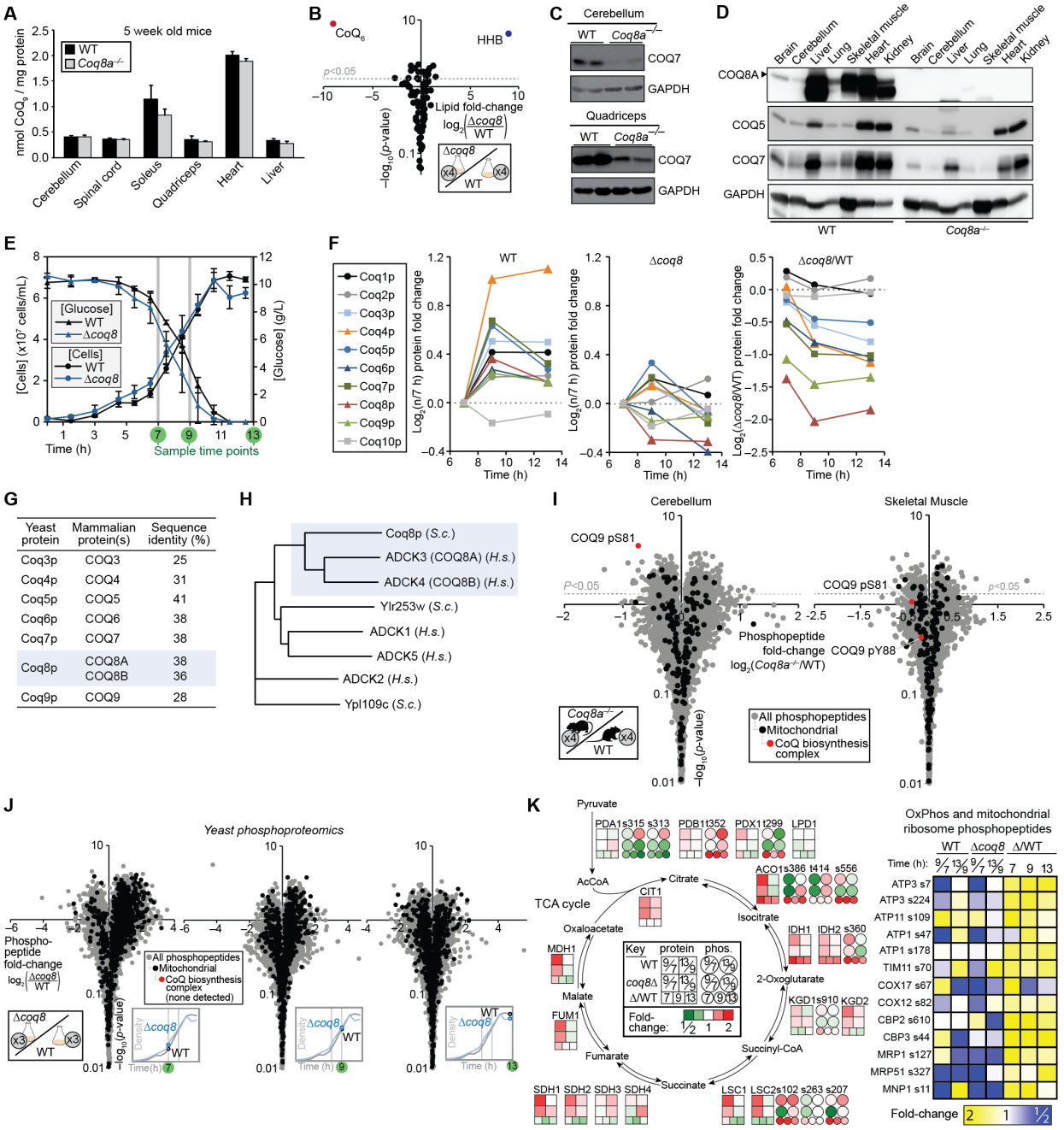

Figure S2, related to Figure 2. Loss of COQ8A or Coq8p Causes Deficiency of Complex Q and CoQ

(A) CoQ_9 abundance in WT and *Coq8a*$^{-/-}$ mice (5-week-old) (mean ± SD, n = 9).

(B) Fold changes in yeast lipid abundances ($\log_2$(Δ*coq8*/WT), mean, n = 3) as quantified by LC-MS analysis. The major yeast CoQ species (CoQ_6) is shown in red, and a CoQ biosynthesis intermediate (HHB, hexaprenylhydroxybenzoate) is shown in blue.

(C) Expression of COQ7 protein in cerebellum (top) and quadriceps (bottom) of WT and *Coq8a*$^{-/-}$ mice (2.5-week-old) as assessed by immunoblot.

(D) Immunoblot analysis of COQ8A, COQ5, and COQ7 abundances across several tissues of 30-week-old mice. Blot is representative of 3 independent biological replicates.

(E) Yeast culture (Δ*coq8* and WT) densities (mean ± SD, n = 3) and glucose concentrations (mean ± SD, n = 3) versus time. Samples were harvested for proteomics and phosphoproteomics analyses at the indicated time points (7 h, 9 h, and 13 h).
(F) Left: Fold changes in CoQ biosynthesis protein abundances in WT or Δ*coq8* yeast ($\log_2$(abundance at indicated time point/abundance at 7 h time point), mean, n = 3) versus time as determined by LC-MS/MS. Right: Fold changes in CoQ biosynthesis protein abundances ($\log_2$(Δ*coq8*/WT), mean, n = 3) at each of the 3 sample time points shown in (E).
(G) Table of yeast and mammalian complex Q proteins indicating amino acid sequence identities for homologous pairs.
(H) Phylogenetic relationship between *Homo sapiens* (*H.s.*) and yeast *Saccharomyces cerevisiae* (*S.c.*) UbiB family proteins.
(I) Fold changes in mouse cerebellum or quadriceps (skeletal muscle) phosphopeptide abundances (mean $\log_2$(*Coq8a*$^{-/-}$/WT), n = 4) versus statistical significance (–$\log_{10}$(*p*-value)) as quantified by LC-MS/MS. Phosphopeptides of mitochondrial proteins are shown in black, and all observed phosphopeptides from CoQ biosynthesis complex proteins are shown in red.
(J) Fold changes in yeast phosphopeptide abundances (mean $\log_2$(Δ*coq8*/WT), n = 3) at the 7, 9, and 13 hour time points versus statistical significance (–$\log_{10}$(*p*-value)) as quantified by LC-MS/MS. Mitochondrial phosphopeptides are shown in black. No phosphopeptides from CoQ biosynthesis complex proteins were observed. Details of the corresponding yeast growth curve and sample time points are shown in (E).
(K) Left: heat maps of fold changes in the abundances of yeast proteins and phosphopeptides (mean, n = 3) from central carbon metabolism pathways as determined by LC-MS/MS. Boxes indicate proteins, and circles indicate phosphopeptides from the protein shown immediately to the left. Right: Heat map of fold changes in the abundances of yeast proteins and phosphopeptides (mean, n = 3) from the mitochondrial ribosome and mitochondrial oxidative phosphorylation complexes as determined by LC-MS/MS.

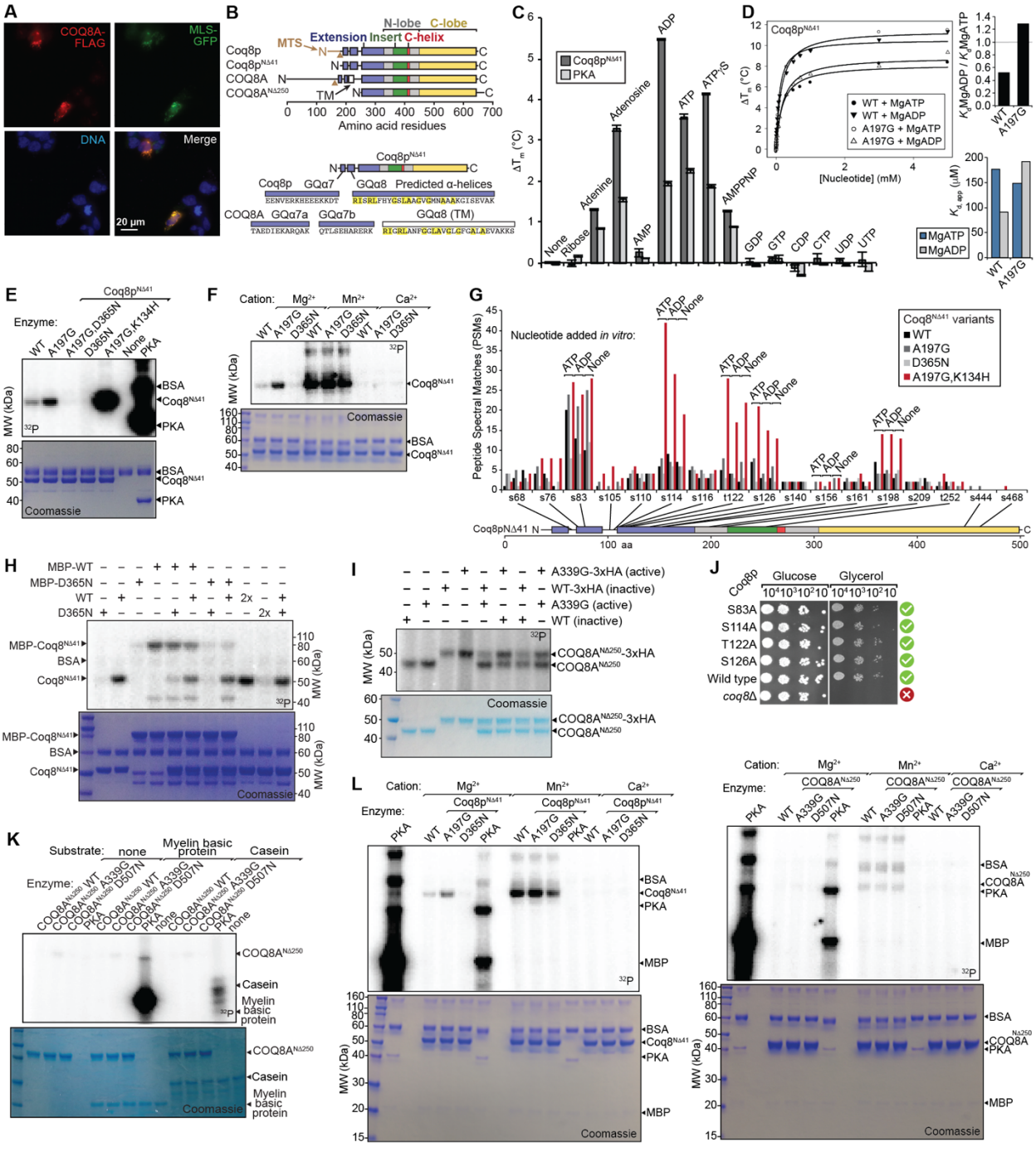

Figure S3, related to Figure 3. Biochemical Activities of COQ8A and Coq8p

(A) Fluorescence microscopy of HEK293 cells transfected with COQ8A-FLAG and MLS-GFP (mitochondrial marker) in parallel with the AE-MS experiment reported here. Nuclear DNA is visualized by Hoechst stain. Scale bar, 20 µm.

(B) Domain structures of Coq8p, COQ8A, and truncated constructs. The white box represents a single-pass transmembrane domain of COQ8A. Brown triangles represent observed N-termini of mature Coq8p and mature COQ8A. MTS, mitochondrial targeting sequence.

(C) ΔT_m of $Coq8^{N\Delta41}$ or PKA due to addition of various ligands (mean ± SD, n = 3) in the presence of Mg^{2+} as assessed by differential scanning fluorimetry (DSF).

(D) Left, nucleotide binding curves for Coq8$^{N\Delta41}$ (WT and A197G). Right, K_d^{MgATP} and K_d^{MgADP} for Coq8$^{N\Delta41}$ (WT and A197G) variants as assessed by DSF, and nucleotide selectivity of Coq8$^{N\Delta41}$ A197G compared to WT.
(E) SDS-PAGE analysis of *in vitro* Mg[γ-^{32}P]ATP autophosphorylation reactions with Coq8$^{N\Delta41}$ variants.
(F) SDS-PAGE analysis of *in vitro* [γ-^{32}P]ATP autophosphorylation reactions with Coq8$^{N\Delta41}$ variants and various divalent cations (Mg^{2+}, Mn^{2+}, or Ca^{2+}).
(G) Number of PSMs observed for Coq8$^{N\Delta41}$ phosphopeptides detected by LC-MS/MS analysis of *in vitro* MgATP autophosphorylation reactions.
(H) SDS-PAGE analysis of *in vitro* Mg[γ-^{32}P]ATP autophosphorylation reactions with the indicated combinations of Coq8$^{N\Delta41}$ variants and maltose binding protein (MBP) tagged Coq8$^{N\Delta41}$ variants.
(I) SDS-PAGE analysis of *in vitro* Mg[γ-^{32}P]ATP autophosphorylation reactions with the indicated combinations of COQ8A$^{N\Delta250}$ variants and 3xHA-tagged COQ8A$^{N\Delta250}$ variants.
(J) Serial dilutions of Δ*coq8* yeast transformed with the indicated *coq8* (Coq8p) variants grown on agar plates with glucose or glycerol.
(K) SDS-PAGE analysis of *in vitro* Mg[γ-^{32}P]ATP kinase reactions with PKA or COQ8A$^{N\Delta250}$ (WT, A339G, or D507N) and potential substrate proteins (myelin basic protein or dephosphorylated casein).
(L) SDS-PAGE analysis of *in vitro* [γ-^{32}P]ATP kinase reactions with PKA, Coq8$^{N\Delta41}$ variants, or COQ8A$^{N\Delta250}$ variants, the generic protein kinase substrate dephosphorylated myelin basic protein (MBP), and various divalent cations (Mg^{2+}, Mn^{2+}, or Ca^{2+}).

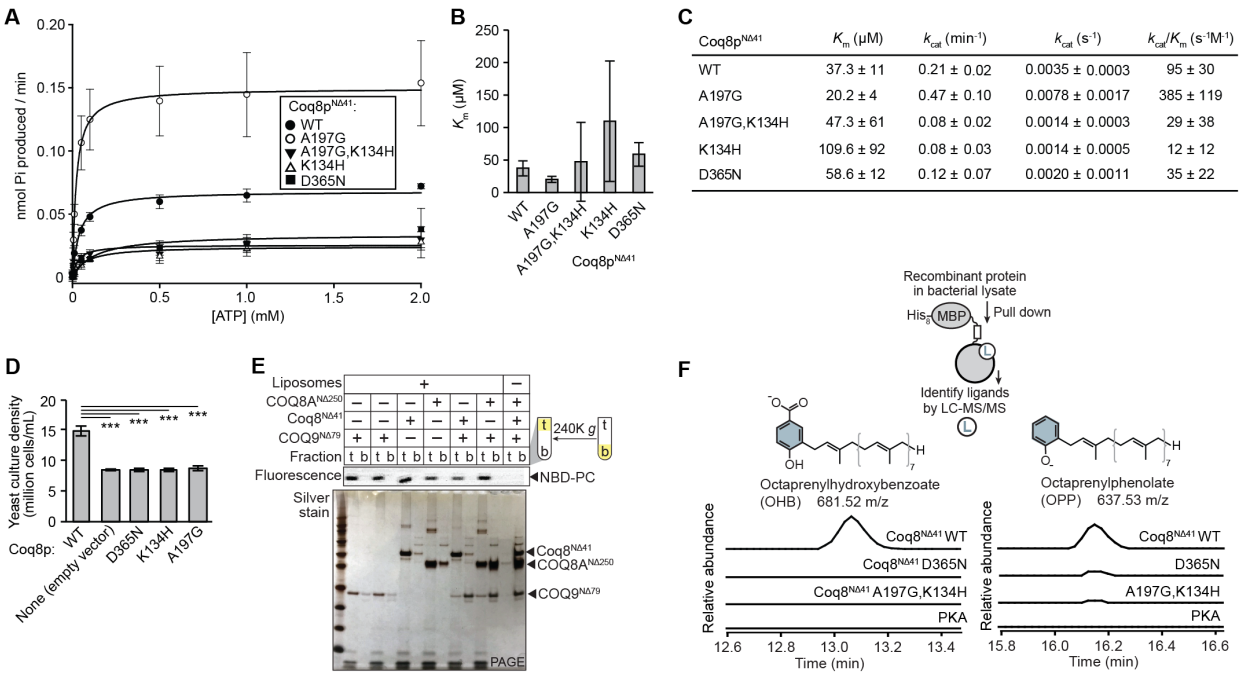

Figure S4, related to Figure 4. Unorthodox PKL Functions of COQ8A and Coq8p

(A) Kinetic curves for the ATPase activity of Coq8$^{N\Delta41}$ variants (WT and mutants) (mean ± SD, n = 3) as measured by observing production of inorganic phosphate (ELIPA assay).

(B) K_m^{MgATP} values for the ATPase activity of Coq8$^{N\Delta41}$ variants (mean ± SD, n = 3).

(C) Table of kinetic constants for the ATPase activity of Coq8$^{N\Delta41}$ variants (mean ± SD, n = 3).

(D) Densities of yeast cultures (Δ*coq8* yeast transformed with plasmids encoding the indicated Coq8p variants) at the time point of harvest for label free quantitation (LFQ) LC-MS/MS proteomics analysis (mean ± SD, n = 4). ***P<0.001.

(E) SDS-PAGE analysis of a liposome-protein co-flotation assay with the indicated proteins and liposomes generated from bacterial extract lipids. The liposomes included a fluorescent lipid marker (NBD-PC). Top (t) and bottom (b) fractions after the spin are indicated.

(F) Extracted ion chromatograms (XICs) reflecting the MS^1 precursor intensities of octaprenylhydroxybenzoate (OHB) and octaprenylphenolate (OPP) that co-purified with MBP- Coq8$^{N\Delta41}$ expressed in *E. coli*. The y-axis (reflecting precursor intensity) for each species is on the same scale across all four proteins.

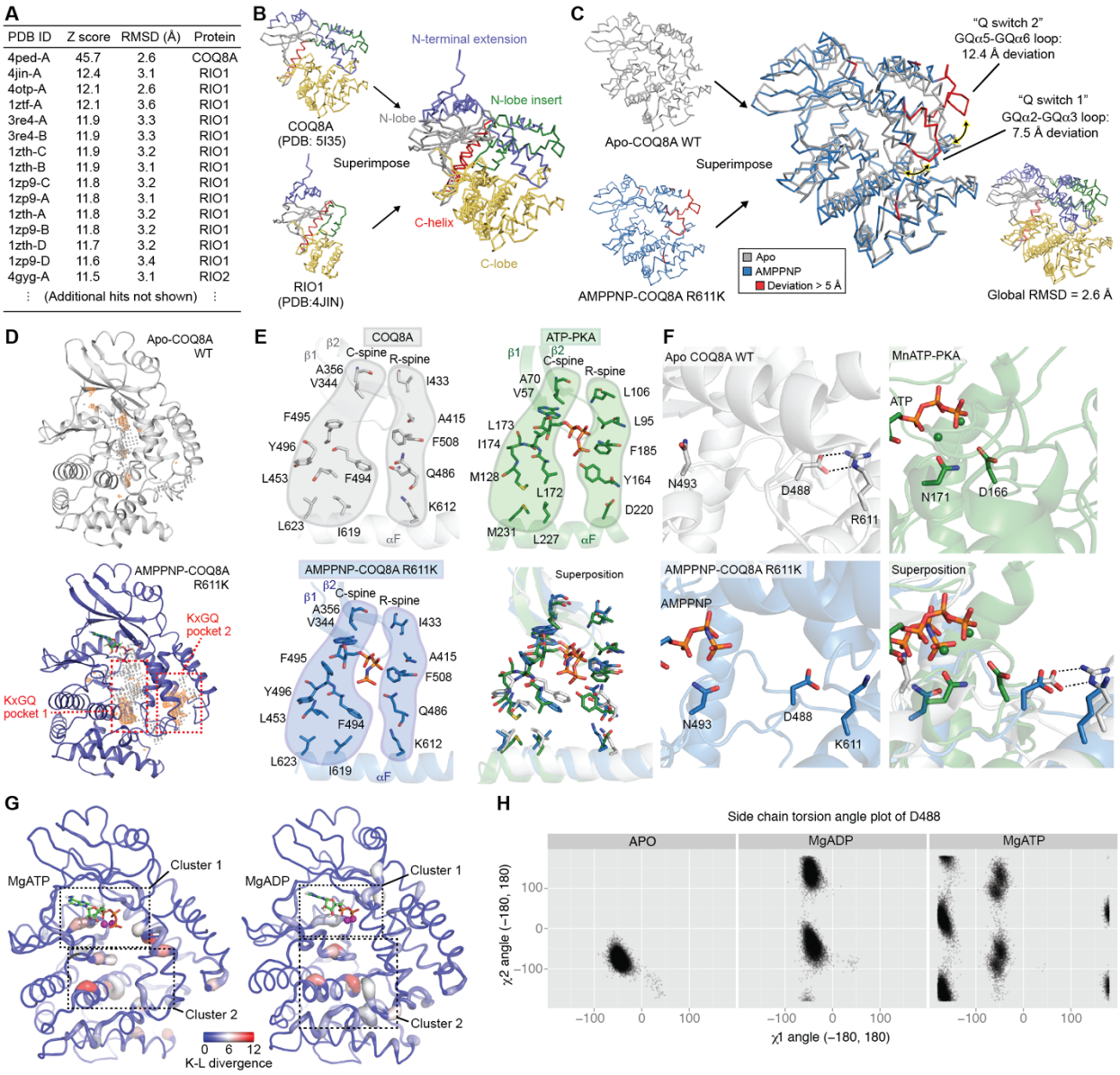

Figure S5, related to Figure 5. Structure and Dynamics of Nucleotide-Bound COQ8A

(A) Structures in the Protein Data Bank (PDB) with the most similarity to AMPPNP-COQ8A$^{N\Delta254}$ R611K (PDB 5I35). The top 15 hits identified with the Dali server (Holm et al., 2008) are shown.

(B) Superposition of AMPPNP-COQ8A$^{N\Delta254}$ R611K (PDB 5I35) and RIO1 (PDB 4JIN).

(C) Superposition of apo-COQ8A WT (PDB 4PED) and AMPPNP-COQ8A R611K (PDB 5I35) indicating in red residues that differ in position by more than 5 Å. The smaller inset superposition (bottom right) is colored by domain as shown in Figures 5A and S3B.

(D) Top-two ranking binding pockets identified by SiteMap on the nucleotide-bound COQ8A structure (PDB 5I35) (blue) and the corresponding pockets on the apo COQ8A structure (PDB 4PED) (gray). The accessible areas of the pockets are shown with white beads, and the hydrophobic regions are shown in orange mesh.

(E) Superposition of "catalytic spine" (C-spine) and "regulatory spine" (R-spine) residues in apo-COQ8A WT (PDB 4PED), AMPPNP-COQ8A R611K (PDB 5I35), and PKA (PDB 1ATP).

(F) Superposition of highly conserved catalytic loop residues in apo-COQ8A WT (PDB 4PED), AMPPNP-COQ8A R611K (PDB 5I35), and PKA (PDB 1ATP).

(G) Kullback–Leibler divergence scores for molecular dynamics (MD) simulations of apo COQ8A compared to MgATP-bound COQ8A (left) or MgADP-bound COQ8A (right). Regions colored red showed highly differential dynamics.
(H) Side chain χ1 and χ2 angle plots of D488 during the MD simulations.

SUPPLEMENTAL TABLE LEGENDS

Table S1. *Coq8a*$^{-/-}$ Mouse Lipidomics, Related to Figure 2B
Table of lipids identified and quantified by LC-MS/MS including lipid name, precursor (MS1) mass, retention time (RT (min)), total signal normalized lipid intensity ([lipid intensity]/[sum of lipid intensities]) for four KO (*Coq8a*$^{-/-}$) mice and four WT mice, average lipid fold change ($\log_2$(*Coq8a*$^{-/-}$/WT)), and $-\log_{10}$(*p*-value). Separate tabs are included for quadriceps, cerebellum, and serum.

Table S2. Δ*coq8* Yeast Lipidomics, Related to Figure S2B
Table of lipids identified and quantified by LC-MS/MS including lipid name, precursor (MS1) mass, retention time (RT (min)), total signal normalized lipid intensity ([lipid intensity]/[sum of lipid intensities]) for four KO (Δ*coq8*) cultures and four WT cultures, average lipid fold change ($\log_2$(Δ*coq8*/WT)), and $-\log_{10}$(*p*-value).

Table S3. *Coq8a*$^{-/-}$ Mouse Proteomics, Related to Figure 2C
Table of proteins identified and quantified by LC-MS/MS including protein description, UniProt ID, gene name, mean normalized log2 fold changes (log2(sample/mean)) for each sample, average protein fold change ($\log_2$(*Coq8a*$^{-/-}$/WT)) (n = 4 WT and 4 KO), and $-\log_{10}$(*p*-value). Separate tabs are included for cerebellum, quadriceps, heart, and kidney.

Table S4. Δ*coq8* Yeast Proteomics, Related to Figure 2F
Table of proteins identified and quantified by LC-MS/MS including protein description, UniProt ID, gene name, mean normalized log2 fold changes (log2(sample/mean)) for each sample, average protein fold changes for each of the three time points (7, 9, and 13 h; before, during, and after the diauxic shift) ($\log_2$(Δ*coq8*/WT)) (n = 3 WT and 3 KO), and $-\log_{10}$(*p*-value) for each time point comparison.

Table S5. *Coq8a*$^{-/-}$ Mouse Phosphoproteomics, Related to Figure S2I
Table of protein phosphosites identified and quantified by LC-MS/MS including protein UniProt ID, protein description, phosphosite(s), average phosphosite fold change ($\log_2$(*Coq8a*$^{-/-}$/WT)) (n = 4 WT and 4 KO), and $-\log_{10}$(*p*-value). Separate tabs are included for quadriceps and cerebellum.

Table S6. Δ*coq8* Yeast Phosphoproteomics, Related to Figures S2J and S2K
Table of protein phosphosites identified and quantified by LC-MS/MS including protein description, phosphosite, UniProt ID, gene name, mean normalized log2 fold changes (log2(sample/mean)) for each sample, average phosphosite fold changes for each of the three time points (7, 9, and 13 h; before, during, and after the diauxic shift) ($\log_2$(Δ*coq8*/WT)) (n = 3 WT and 3 KO), and $-\log_{10}$(*p*-value) for each time point comparison.

SUPPLEMENTAL EXPERIMENTAL PROCEDURES

Coq8a$^{-/-}$ Mice

Generation of Coq8a$^{-/-}$ *Mice*. Mice carrying a conditional allele for *Coq8a*$^{L2+/L2+}$ were established at the MCI/ICS (Mouse Clinical Institute – Institut Clinique de la Souris-Phenomin, Illkirch, France). The conditional allele was generated by inserting two loxP sites into introns 9 and 15 of the *Coq8a (Adck3)* locus (see Figure S1A). The targeting vector was constructed as follows. A 1.9 kb fragment encompassing exons 9, 10, 11, 12, 13 and 14 was amplified by PCR (from 129S2/SvPas ES cells genomic DNA) subcloned in an MCI proprietary vector. This MCI vector contains a LoxP site as well as a floxed and flipped Neomycin resistance cassette. A 4.5 kb fragment (corresponding to the 5' homology arm and 3.5 kb fragment corresponding to the 3' homology arms were amplified by PCR and subcloned in step 1 plasmid to generate the final targeting construct.

The linearized construct was electroporated in 129S2/SvPas mouse embryonic stem (ES) cells. After selection, targeted clones were identified by PCR using external primers and further confirmed by Southern blot with 5' and 3' external probes.

Two positive ES clones were injected into C57BL/6J blastocysts, and male chimaeras derived gave germline transmission. After expression of Cre recombinase under the CMV promoter, a deletion of exons 9–14 was obtained that constitutes the constitutive knockout *Coq8a*$^{-/-}$ (*Adck3*$^{-/-}$) allele. Mice were analyzed in a mixed background (Bl/6J 53.13%, Bl/6N 34.37%, 129svPas 12.5%). Because we did not find any significant difference between WT and *Coq8a*$^{+/-}$ heterozygotes, we considered heterozygotes as controls for some behavioral and histological experiments.

Genotyping. To genotype mice, DNA (mouse tail) was examined by PCR with the following primers:

Wild type (WT) allele: 5'-CTTTCAGTTTTTAGTACTGGCTGCG-3',
5'-GCTCATTAGTGTCCCAGCCATATCC-3';
Coq8a$^{-/-}$ (KO) allele: 5'-CTTTCAGTTTTTAGTACTGGCTGCG-3',
5'-AGAGCACTGGAGGGACAAGGGGC-3'.

General Handling. Mice were maintained in a temperature and humidity controlled animal facility, with a 12 hours light/dark cycle and free access to water and a standard rodent chow (D03, SAFE, Villemoisson-sur-Orge, France). All animal procedures and experiments were approved by the local ethical committee for Animal Care and Use (Com'Eth n° 2012-154) and were performed in accordance with the Guide for the Care and Use of Laboratory Animals (National Institutes of Health).

Blood Analysis. Blood was collected by retro orbital puncture under isoflurane anesthesia after 4 hr fasting at the age of 25 weeks. Blood chemistry was examined using an OLYMPUS AU-400 automated laboratory work station (Olympus France SA, Rungis, France) using commercial reagents (Olympus Diagnostica GmbH, Lismeehan, Ireland).

Mammalian Cell Culture

Primary Myoblasts. Hind limb muscle from 7–9-day-old mice was collected, minced and digested with a mixture of collagenase and dispase (Invitrogen). The digestions were stopped with growth medium containing Iscove's Modified Dulbecco's Medium (IMDM, Gibco), centrifuged (600 *g,* 5 min), filtered, and centrifuged again (1300 *g*, 5 min). The cell pellet was suspended in IMDM supplemented with 10% fetal bovine serum (FBS), 2 mM L-glutamine, and 0.1% gentamycin, and plated into 6-well dishes. Myoblasts were separated from fibroblast contaminants by differential plating for 3–4 hours in an incubator. The cells were subsequently centrifuged (1,500 *g*, 10 min) and plated on matrigel-coated dishes in IMDM supplemented with 20% FBS, 2 mM L-Gln, 1% Chicken Embryo Extract (Seralab), and 0.1% gentamycin. The cells were maintained in an incubator (37 °C, 5% CO_2) and the medium was changed every 2 days.

COS Cells. COS cells were maintained in DMEM supplemented with 5% FBS in a humidified incubator (37 °C, 5% CO_2). Transfections were conducted as described below in the protein interaction method section.

HEK293 Cells. HEK293 cells were maintained in high glucose (25 mM) Dulbecco's modified Eagle's medium (LifeTech) supplemented with 10% (v/v) FBS (LifeTech) and penicillin-streptomycin (1×) (LifeTech) (HGDMEM+FBS+P/S) in a humidified incubator (37 °C, 5% CO_2). Cells were sub-cultured by trypsinization (0.05% Trypsin-EDTA, LifeTech). Transfections were conducted as described below in the protein interaction method section.

Yeast Cultures

Yeast cultures for lipidomics and diauxic shift proteomics and phosphoproteomics. Saccharomyces cerevisae WT strain DS10 was obtained from the laboratory of Elizabeth A. Craig ("WT JH27a DS10", *his3-11,15 leu2-3,112 lys1 lys2 Δtrp1 ura3-52*). Δ*coq8* DS10 yeast were created by replacing the *coq8* gene with a *ura3* selectable marker using

standard methods for PCR amplification and homologous recombination (Baudin et al., 1993). The insertion of the *ura3* marker at the *coq8* locus was confirmed by a PCR assay and DNA sequencing. Single colonies of yeast were used to inoculate starter cultures in YPD media (4 mL), which were incubated (30 °C, 230 rpm, 12 h). Synthetic complete media (500 mL) with glucose (10 g/L) was inoculated with $5x10^6$ yeast cells from a starter culture and incubated (30 °C, 230 rpm). Yeast cell pellets were isolated at three time points during the culture (as shown in Figure S2E) by centrifugation (1,000 *g*, 3 min, 4 °C) and frozen in $N_{2(l)}$. Cell culture density was determined by measuring the optical density at 600 nm (OD_{600}) and converting this value to [cells], as described previously (Hebert et al., 2013). Media glucose concentration was determined with a Glucose (HK) Assay Kit (Sigma), as described previously (Hebert et al., 2013).

Yeast cultures for drop assays. *S. cerevisiae* (W303) Δ*coq8* yeast were transformed as previously described (Gietz and Woods, 2002) with p426 GPD plasmids encoding Coq8p variants and grown on uracil drop-out (Ura^-) synthetic media plates containing glucose (20 g/L). Individual colonies of yeast were used to inoculate Ura^- media (20 g/L glucose) starter cultures, which were incubated (30 °C, ~18 h, 230 rpm). Serial dilutions of yeast (10^4, 10^3, 10^2, or 10 yeast cells) were dropped onto Ura^- agar media plates containing either glucose (20 g/L) or glycerol (30 g/L) and incubated (30 °C, 2 d).

Yeast cultures for LFQ proteomics of coq8 point mutant strains. S. cerevisiae (BY4742) Δ*coq8* yeast were transformed with p426 GPD plasmids encoding Coq8p variants and grown on Ura^- synthetic media plates (20 g/L glucose). Individual colonies of yeast were used to inoculate Ura^- media (20 g/L glucose) starter cultures, which were incubated (30 °C, ~12 h, 230 rpm). 100 mL cultures (Ura^- media with 30 g/L glycerol and 1 g/L glucose) were inoculated with 2.5 million yeast and incubated (30 °C, 230 rpm, 25 h). $1x10^8$ yeast cells were harvested by centrifugation (3,000 *g*, 3 min, 4 °C), the supernatant was removed, and cell pellets were flash frozen in $N_{2(l)}$.

DNA Constructs and Cloning

General Cloning Methods. Standard PIPE cloning methods (Klock et al., 2008) were used where indicated. PIPE reactions were DpnI digested and transformed into DH5α competent *E. coli* cells. Plasmids were isolated from transformants and DNA sequencing was used to identify those containing the correct constructs. pVP68K, a plasmid for expression of recombinant proteins in bacteria [8His-cytoplasmically-targeted maltose-binding protein (MBP) with a linker including a tobacco etch virus (TEV) protease recognition site fused to the protein construct (8His-MBP-[TEV]-Protein)], has been described previously (Blommel et al., 2009). Oligonucleotides were purchased from IDT (Coralville, IA, USA).

Human COQ8A^{NΔ250}-FLAG-3xHA (ADCK3^{NΔ250}-FLAG-3xHA). Cloning of COQ8A^{NΔ250} (ADCK3^{NΔ250}) into pVP68K has been described previously (Stefely et al., 2015). Here, to generate COQ8A^{NΔ250}-Flag-3xHA with PIPE cloning, separate COQ8A^{NΔ250} and FLAG-3xHA amplicons were generated and combined prior to transformation. The 3xHA was amplified from plasmid pJR13019 (Chen et al., 2012), obtained from the laboratory of Jared Rutter. Point mutations were introduced by PCR-based mutagenesis and confirmed by DNA sequencing.

Murine PKA. pET15b PKA Cat (Narayana et al., 1997) was obtained as a gift from Susan Taylor (Addgene plasmid #14921), and PKA was PIPE cloned into pVP68K. Point mutations were introduced by PCR-based mutagenesis and confirmed by DNA sequencing.

Yeast Coq8^{NΔ41}. *S. cerevisiae coq8* was PIPE cloned into pVP68K and the N-terminal 41 amino acid residues were removed by standard PIPE cloning methods. Point mutations were introduced by PCR-based mutagenesis and confirmed by DNA sequencing.

Yeast Coq8. Cloning of *S. cerevisiae coq8* into the yeast expression vector p426 GPD has been described previously (Stefely et al., 2015). Point mutations were introduced by PCR-based mutagenesis and confirmed by DNA sequencing.

Human COQ8A-FLAG (ADCK3-FLAG). Cloning of human COQ8A-FLAG (ADCK3-FLAG) (C-terminal FLAG tag) into pcDNA3.1 has been described (Stefely et al., 2015). Point mutations were introduced by PCR-based mutagenesis and confirmed by DNA sequencing.

Murine Coq8a-FLAG (Adck3-FLAG), Coq3-HA, Coq5-HA, and Coq9-HA. The complete coding sequence of murine *Coq8a* (*Adck3*) was cloned into the pcDNA 3.1/Zeo (Invitrogen) expression vector with a C-terminal FLAG tag. Similarly, full-length murine *Coq3*, *Coq5*, and *Coq9* were cloned into the pcDNA 3.1/Zeo vector with a C-terminal HA tag.

Antibodies and Western Blots (Immunoblots)

Anti-Coq8a Antibody. An anti-Coq8a antibody (targeting the murine COQ8A protein) was generated in-house (IGBMC) against the following peptide: KQMTKTLNSDLGPHWRDKC. The peptide was conjugated to Keyhole limpet hemocyanin (KLH) using Imject Maleimide Activated mcKLH kit (Thermo Scientific, Rockford, USA)

according to the manufacturer's recommendations and then injected with complete Freund's adjuvant into white New Zealand rabbits according to standard procedure. The antibody was purified from serum by affinity chromatography using the SulfoLink Coupling Resin (Thermo Scientific) and PolyPrep Chromatography Columns (Biorad). The antibody was eluted in acidic elution buffer (0.1 M glycine pH 2.8) followed by dialysis of the antibody-containing fractions overnight against PBS (1 L filtered PBS). The reactivity of the antibody with COQ8A in a panel of different cell and tissue lysates was then evaluated by Western blot.

Western blots. Western blots (immunoblots) were performed according to standard protocol, including separation of proteins by SDS Tris-Glycine PAGE. Antibodies were diluted as follows: anti-GAPDH (1/40000, Millipore), anti-COQ7 (1/1000, Abcam), anti-COQ5 (Proteintech 17453-1-AP, 1/1000), anti-Prohibitin (1/1000, Neo Markers), anti-TOM20 (1/250, Santa Cruz Biotechnology), anti-CYC1 (Proteintech), anti-NFU1 (1/5000, a gift from Tracey Rouault, National Institutes of Health), anti-FLAG 1/1000, and anti-HA 1/1000. HRP-coupled secondary antibodies (Horseradish Peroxidase, Jackson Immuno Research) were diluted at 1/5000.

Behavioral Measurements

Accelerating Rotarod. Coordination, balance, and motor skill acquisition were tested using an accelerating rotating rod (Panlab, Barcelona, Spain) test as described previously (Clark et al., 1997). Briefly, mice were placed on the rod in 4 trials every day for a period of 4 days (10 WT and 10 *Coq8a*$^{-/-}$ mutants). The rod accelerated from 4 rpm to 40 rpm in 5 min and remained at maximum speed for the next 5 min. Animals were scored for their latency to fall for each trial and rested a minimum of 10 min between trials to avoid fatigue. Results were analyzed by a repeated-measure ANOVA test considering three factors: days (fixed); genotype (fixed); animals (variable), nested in genotype and crossed with days.

Footprint Analysis (Linear Movement). The test was performed as previously described (Simon et al., 2004). Briefly, after coating of the hind feet with nontoxic ink, mice were allowed to walk through a tunnel (50×9×6 cm) with paper lining the floor. Five parameters were quantified: step length, the average distance of forward movement between alternate steps; σ, describing the regularity of step length; gait width, the average lateral distance between opposite left and right steps; alternation coefficient, describing the uniformity of step alternation; linearity, average change in angle between consecutive right-right steps. A high linearity score is indicative of nonlinear movement.

Beam-Walking (Hindlimb Coordination). Mice were trained to walk along a beam (2 cm wide × 90 cm long) suspended 30 cm above bedding. Three trials were performed for each mouse, and the number of hindfoot missteps was counted while the mouse walked along the length of the beam. The time required to cross the beam from start to end (latency) was also evaluated. Mice were trained to walk the length of the beam 1 day before testing

PTZ-Induced Seizures. Pentylenetetrazole (PTZ) was dissolved in saline (0.9% NaCl) and intraperitoneal (IP) injected at a dose of 30 mg/kg. Immediately after injection, the mouse was placed into a new cage and observed for at least 20 min. The seizure profile (myoclonic, clonic, tonic) and the latency to clonico-tonic seizure were recorded.

Y-Maze Spontaneous Alternation. A Y-maze made of Plexiglas with 3 identical arms (40×9×16 cm) placed 120° from each other was used for this test. Each arm had walls with distinct motifs allowing it to be distinguished from the others. Each mouse was placed at the end of one of the three arms, and allowed to explore freely the apparatus for 5 min, with the experimenter out of the animal's sight. Alternations were operationally defined as successive entries into each of the three arms as overlapping triplet sets (i.e., ABC, BCA...). The percentage of spontaneous alternation was calculated as index of working memory performance. Total arm entries and the latency to exit the starting arm were also scored as indexes of ambulatory activity and emotionality in the Y-maze, respectively.

Object recognition task: The object recognition task was performed in automated open fields (45×45×18 cm). The open fields were placed in a room homogeneously illuminated at 70 Lux at the level of each open field. The objects to be discriminated were a glass marble (2.5 cm diameter) and a plastic dice (2 cm). Animals were first habituated to the open field for 30 min. The next day, they were submitted to a 10 min acquisition trial during which they were placed in the open field in presence of an object A (marble or dice). The time the animal took to explore the object A (when the animal's snout was directed towards the object at a distance ≤ 1 cm) was manually recorded. A 10 min retention trial was performed 3 h later. During this trial, the object A and another object B were placed in the open field, and the times tA and tB the animal took to explore the two objects were recorded. The recognition index (RI) is defined as (tB / (tA + tB))×100.

Morris Water Maze. The water maze consisted of a white circular tank (1.5 m diameter) filled with opaque water. Pool temperature was adjusted to 21±1 °C. For the hidden platform task, the escape platform (10 cm diameter) was positioned 1 cm below water level in the center of one of the pool quadrants. For the cued task, platform position was signaled by the addition of a small flag. The walls surrounding the water maze were hung with posters and flags, which served as visual cues and are visible during all stages of training and testing. Movement of the mice within the pool was tracked and analyzed with a computerized tracking system (ViewPoint, France). Animals were first trained

in the hidden platform protocol (spatial learning). Mice were required to locate a submerged hidden platform by using only extra-maze cues. Each mouse received 5 blocks of training trials over five consecutive days in which they were placed in the pool at one of four randomized start positions, and allowed to locate the hidden platform. Trials lasted for a maximum of 120 s and were separated by 15–20 min intervals. If a mouse failed to find the platform within this period, it is guided to its position by the experimenter. Spatial learning performance was assessed during a probe trial 1 h after training, and for which the target platform was removed from the pool. Mice were then tested for cued training (visible platform), in which they were placed in the pool facing the edge at one of four start positions (NE, SE, SW, NW), and required to locate a flagged platform whose position varies across trials. Each mouse received 4 trials per day for 2 consecutive days. Trials lasted for a maximum of 120 s and were separated by 15–20 min intervals. If a mouse failed to find the platform within this period, it is guided to its position by the experimenter. The latency, distance and the average speed were used to evaluate performance during training trial. For the probe trial, the percentage of time in each quadrant and the number of platform crosses were used as index of spatial learning performance.

Treadmill. Mice were run on a treadmill with a 10° slope. Two protocols were applied: (i) for the V_{max} test, the starting speed of 40 cm/sec was increased 3 cm/sec every 90 seconds up to exhaustion. (ii) For the endurance test, mice were run until exhaustion at 80% of their respective V_{max}. Exhaustion of the mice was verified by blood lactate measurement.

Grip Test. Mice placed on the grid of a dynamometer (BioSeb, Chaville, France) were pulled by their tails in the opposite direction. The maximal strength exerted by the mouse before losing grip was recorded. The mean of 3 measurements allowing 30 sec of recovery time was calculated.

Microscopy

Immunohistochemistry. Animals were intracardiac perfused with 4% paraformaldehyde (PFA) in phosphate buffered saline (PBS), pH 7.3, and the various tissues were dissected, fixed for several days, and embedded in paraffin. Sequential slides (7 µm) of the paraffin blocks were stained with hematoxylin and eosin (H&E), or calbindin (1:1000; rabbit anti-calbindin d-28K; Swant, Bellinzona, Switzerland) to label the cytoplasm of Purkinje cells. For calbindin staining, sections were visualized using the Vectastain ABC Kit (Vector Laboratories, Burlingame, CA) as described in the manufacturer's protocol. Quantification of Purkinje cells was performed in a blinded manner. Images of the Purkinje cell layers were taken with a 20× objective. 3 mice per genotype and 10 images per mouse were included in the analysis.

Electron Microscopy. Animals were intracardiac perfused with 4% PFA. Tissues were fixed in 2.5% glutaraldehyde in PBS. After overnight fixation, the tissues was dissected from the column and fixed for 1 additional day. Tissues were rinsed in PBS, postfixed in 1% osmium tetroxide-PBS (2 hr, 4 °C), dehydrated, and embedded in Epon. Regions of interest were localized on 2 µm sections and stained with toluidine blue. Ultrathin sections from selected areas were stained with uranyl acetate and lead citrate and examined with a Philips 208 electron microscope, operating at 80 kV.

TUNEL Assay. Apoptosis was assessed by the *in situ* DNA end-labeling [terminal deoxynucleotidyl transferase-mediated biotinylated UTP nick end labeling (TUNEL)] method, following the manufacturer's directions (Apoptag, Intergen Co., Purchase, NY). Purkinje cells were blindly counted on H&E sections. 9–11 images were taken per cerebellum and 3 mice per genotype were considered in the analysis.

PCR Assays

Purkinje Cell Markers and Coq8 Expression. Total RNA was extracted from frozen tissues with the Precellys24 homogeniser (Bertin Technologies) and using TRI Reagent (MRC) according to the manufacturer's protocol. cDNA was generated by reverse transcription using the Transcriptor First strand cDNA synthesis kit (Roche). Quantitative RT-PCR was performed using the SYBR Green I Master (Roche) and light Cycler 480 (Roche) with the primers described below. *Gapdh* or *Hprt* was used as internal standard for the quantification.

Pcp2: ACAGTTAATTCCCTGCCTGG and CTCAAGGAGCTTGTGTCTGG
Calb1: GATTGGAGCTATCACCGGAA and TTCCTCGCAGGACTTCAGTT
Gapdh: TTGTGATGGGTGTGAACCAC and TTCAGCTCTGGGATGACCTT
Hprt: GTAATGATCAGTCAACGGGGGAC and CCAGCAAGCTTGCAACCTTAACCA
Coq8a: TCATATCAGGCTTCCCCTTG and TTCTCTAGTTGCGCCGAAGT
Coq8b : ATGGTCCGTGAACTCTGTCC and TGCTTTCAGCTCCTGAGGTT

Quantification of mtDNA copy number. Mitochondrial DNA (mtDNA) copy number was determined as a marker for mitochondrial density using quantitative real time PCR. Total DNA was extracted from frozen tissues that were lysed overnight at 55 °C in NaCl 200 mM, Tris 50 mM pH 8, EDTA 5 mM, SDS 1% in the presence of 100

µg/mL proteinase K. The next day, RNAse treatment (3 mg/mL) was performed at 37 °C for 30 min, before extraction of total DNA using standard phenol/chloroform treatment followed by DNA precipitation. Quantitative PCR was performed using the Light Cycler 480 II (Roche, France) and the Light cycler 480 SYBR Green I Master (Roche, France). 100 ng of total DNA was used for amplification of genomic DNA, while 1 ng of total DNA was used for amplification of mtDNA. The ND1 gene for NADH dehydrogenase subunit 1 was used for quantification of mtDNA. The nuclear gene for lipoprotein lipase (LPL) was used to normalize results. The ratio of ND1 to LPL copy number reflected the tissue concentration of mitochondria per cell.

Nd1 : CCCAGCTACTACCATCATTCAAGT and GATGGTTTGGGAGATTGGTTGATGT
Lpl : CACAGTGGCCGAGAGCGAGAA and GCTGAGTCCTTTCCCTTCTGCA

Purkinje Cell Electrophysiology

Slice preparation and recordings. Slices were prepared as previously described (Chaumont et al., 2013). Briefly, male *Coq8a*$^{-/-}$ mice and WT littermates (3-month-old and 8-month-old) were decapitated under isoflurane anesthesia. 330 µm-thick sagittal slices were prepared (Microm HM 650V, Microm) in potassium-based medium, containing in mM: K-gluconate 130; KCl 14.6; EGTA 2; Hepes 20; Glucose 25; minocyclin 0.00005, and D-AP5 0.05. Slices were soaked in a sucrose- based medium at 34 °C, containing in mM: sucrose 230; KCl 2.5; $NaHCO_3$ 26; NaH_2PO_4 1.25; glucose 25; $CaCl_2$ 0.8; $MgCl_2$ 8; minocyclin 0.00005; and D-APV 0.05 and transferred for recordings in an artificial cerebrospinal medium (ACSF) containing in mM: NaCl 120; KCl 3; $NaHCO_3$ 26; NaH_2PO_4 1.25; $CaCl_2$ 2.5; $MgCl_2$ 2; Glucose 10; Minocyclin 0.00005 (chemicals from Sigma-Aldrich, USA and Abcam, UK). Extracellular recordings of individually identified Purkinje cells were performed at 32–34 °C in the presence of picrotoxin (100 µM) using 15–30 MΩ pipettes filled with 0.5 M NaCl. Data were recorded using an Axopatch 200A (Molecular Devices, USA) and acquired using WinWCP 4.5.4 freeware (John Dempster, University of Strathclyde, UK). Recordings were filtered at 2 kHz and sampled at 50 kHz.

Analyses. Spike detection was performed using OpenElectrophy (Garcia and Fourcaud-Trocme, 2009) and custom based routines written in Python (Antoine Valera). Discharge regularity was assessed by the CV2 of interspike-intervals (ISI): $CV2=2|ISI_{n+1}-ISI_n|/(ISI_{n+1}+ISI_n)$ (Holt et al., 1996). Student's t-test and the Mann–Whitney U test were used for statistics.

Mitochondria Respiration Analysis

Mice were anesthetized with 300 µL of intraperitoneal injection (10 % pentobarbital solution in 10 mM NaCl). Muscles were collected and placed in S solution (see below). Fibers were separated under a binocular microscope in solution S at 4 °C and permeabilized for 30 min in solution S supplemented with 50 µg/mL of saponin. Isolated fibers were subsequently placed for 10 min in solution R (see below) to wash out adenine nucleotides and creatine phosphate. They were then transferred to a 3 mL water-jacketed oxygraphic cell (Strathkelvin Instruments, Glasgow, UK) equipped with a Clark electrode, as previously described (Jeukendrup et al., 1997). Solutions R and S contained 2.77 mM CaK_2EGTA, 7.23 mM K_2EGTA, 6.56 mM $MgCl_2$, 20 mM taurine, 0.5 mM DTT, 50 mM potassium-methane sulfonate (160 mM ionic strength) and 20 mM imidazole (pH 7.1). Solution S also contained 5.7 mM Na_2ATP, 15 mM creatine-phosphate, while solution R also contained 5 mM glutamate, 2 mM malate, 3 mM phosphate, and 2 mg/mL fatty acid free bovine serum. V_{INIT} was measured in the absence of fibers and substrates at 22 °C under continuous stirring. V_0 corresponds to the rate of O_2 consumption after addition of muscle fibers and glutamate-malate as substrate, to which V_{INIT} is subtracted. V_{MAX} (maximal respiration) corresponds to the rate of O_2 consumption after addition of 2 mM of ADP as a phosphate acceptor, to which V_{INIT} is subtracted. The acceptor control ratio, ACR, is defined as the ratio between V_{MAX} and V_0. After measurement, fibers were dried, and respiration rates were expressed as micromoles of O_2 per minute per mg of dry weight.

Metabolomics Analysis of Mouse Quadriceps Muscle by GC-MS

Metabolite extraction. Mouse quadriceps were rapidly isolated from 31-week-old female mice (4 WT and 4 KO) and frozen in $N_{2(l)}$. Samples of frozen mouse quadriceps (~30 mg of tissue) were homogenized under liquid nitrogen using a mortar and pestle, and the resultant powder of frozen tissue was transferred to a tube with ACN/IPA/H_2O (2:2:1, v/v/v, 1.5 mL, pre-cooled to –20 °C and kept on dry ice). After briefly mixing, the tube was flash frozen in $N_{2(l)}$. Once all of the samples were brought to this point, they were thawed in parallel to 4 °C (still ice cold). The samples were mixed by vortexing (4 °C, 1 min) to complete the extraction. The samples were centrifuged (5,000 *g*, 5 min, 4 °C) to pellet insoluble material. The supernatant was transferred to a new tube (pre-cooled to 4 °C), flash-frozen in $N_{2(l)}$, and store at –80 °C.

Tissue extract sample preparation for GC-MS. Tissue extracts were thawed at room temperature for 1 hour, 150 µL of each were aliquoted into glass autosampler vials along with 10 µL of 1 ppm isotopically labeled alanine-

2,3,3,3-d_4 and adipic acid-d_{10}. Samples were then dried to completion using a vacuum concentrator (1 hour). Once dry, the samples were re-suspended in 50 µL of a 1:1 mixture of pyridine and N-methyl-N-trimethylsilyl]trifluoroacetamide (MSTFA) with 1% trimethylchlorosilane (TMCS). The mixture was vortexed for 10 seconds, and then heated to 60 °C for 30 minutes.

Mass spectrometric analysis. Samples were analyzed using a GC/MS instrument comprising a Trace 1310 GC coupled to a Q-Exactive Orbitrap mass spectrometer (Thermo Fisher Scientific). A temperature gradient ranging from 100 °C to 320 °C was employed spanning a total runtime of 25 minutes. Analytes were injected onto a 30 m TraceGOLD TG-5SILMS column (Thermo Fisher Scientific) at 1 µL volume, using a 1:10 split ratio, at an injector temperature of 275 °C, and the GC effluent subjected to electron ionization (EI). The mass spectrometer was operated in full scan mode using a resolution of 30,000 ($m/\Delta m$) relative to 200 *m/z*.

Mass spectral data analysis. The resulting GC-MS data were processed using an in-house developed software suite (*https://github.com/coongroup*). Briefly, all *m/z* peaks are aggregated into distinct chromatographic profiles (i.e., feature) using a 10 ppm mass tolerance. These chromatographic profiles are then grouped according to common elution apex (i.e., feature group). The collection of features (*i.e.*, *m/z* peaks) sharing a common elution apex, therefore, represent an individual EI-MS spectrum of a single eluting compound. The EI-MS spectra were then compared against a matrix run and a background subtraction was performed. Remaining EI-MS spectra are then searched against the NIST 12 MS/EI library and subsequently subjected to a high resolution filtering (HRF) technique as described elsewhere. EI-MS spectra that were not identified were assigned a numeric identifier. Feature intensity, which was normalized using internal standards and total metabolite signal, was used to estimate metabolite abundance.

Targeted HPLC-EC Quantification of CoQ_9 and CoQ_{10}

Homogenates (5%, w/v) of various organs from 5- and 32-week-old *Coq8a*$^{-/-}$ and WT mice were prepared on ice with an Ultra-Turrax in Tris-HCl 50 mM (pH 7.5) containing 50 mM KCl, 10% glycerol, 1 mM EDTA and 0.2% Triton-X 100. Aliquots were adjusted to 0.5 mL with 0.15 M KCl and extracted with 4.5 mL methanol (MeOH) and 3 mL hexane with vigorous shaking after each addition. Following phase separation, the upper hexane phase was collected and evaporated under $Ar_{(g)}$. The lipid residue was dissolved in ethanol (EtOH) and loaded on an Ultimate 3000 HPLC system (Dionex) at a flow rate of 1 mL/min. Separation was achieved on a Thermo Betabasic-18 column (4.6×150 mm, 5 µm particle size) after oxidization of the sample with an ESA 5020 guard cell (E; +700 mV). The linear gradient started at 25% isopropanol (IPA), 20% MeOH, 55% acetonitrile (ACN) and 10% solvent D (200 mM $LiClO_4$ in IPA:H_2O (85:15, v/v) and ended 20 min later at 30% IPA and 15% MeOH with ACN and solvent D unchanged. Detection was performed with a diode array detector and a Coulochem III detector with an ESA 5011A analytical cell (E1; −700mV E2; +700 mV). CoQ_8 was used as internal standard and calibrated at 275 nm in EtOH. Protein was measured with a BCA kit (Sigma).

Mass Spectrometry-Based Lipidomics

Mouse Tissue Homogenization. Mouse cerebellum and quadriceps tissues (4 biological replicates of *Coq8a*$^{-/-}$ mice and 4 biological replicates of WT mice, 8-month-old) were homogenized in Lipidomics Homogenization Buffer [phosphate (11.8 mM), NaCl (137 mM), KCl (2.7 mM), pH 7.2, phosphatase inhibitors (PhosSTOP, Roche), protease inhibitors (cOmplete, Mini, Roche)] at 4 °C (in a cold room) as quickly as possible (< 5 min).

Cerebellum Lipid Extractions. Mouse cerebellum homogenate (0.65 mg protein, 280 µL) was spiked with an internal standard (CoQ_6, 20 µL, 10 µM) and mixed by vortexing (30 s). $CHCl_3$/MeOH (1:1, v/v) (900 µL) was added and vortexed (2 × 30 s). HCl (1 M, 100 µL, 4 °C) was added and vortexed (2 × 30 s). The samples were centrifuged (3,000 *g*, 3 min, 4 °C) to complete phase separation. 500 µL of the lower organic phase was transferred to a clean tube and dried under $Ar_{(g)}$. The organic residue was reconstituted in ACN/IPA/H_2O (65:30:5, v/v/v) (100 µL) by vortexing (2 × 30 s).

Quadriceps Lipid Extractions. Mouse quadriceps homogenate (1 mg protein, 250 µL) was spiked with an internal standard (CoQ_6, 20 µL, 10 µM) and mixed by vortexing (30 s). $CHCl_3$/MeOH (1:1, v/v) (900 µL) was added and vortexed (2 × 30 s). HCl (1 M, 100 µL, 4 °C) was added and vortexed (2 × 30 s). The samples were centrifuged (3,000 *g*, 3 min, 4 °C) to complete phase separation. 500 µL of the lower organic phase was transferred to a clean tube and dried under $Ar_{(g)}$. The organic residue was reconstituted in ACN/IPA/H_2O (65:30:5, v/v/v) (100 µL) by vortexing (2 × 30 s).

Serum Lipid Extractions. Mouse serum (90 µL) was spiked with an internal standard (CoQ_6, 20 µL, 10 µM) and mixed by vortexing (30 s). $CHCl_3$/MeOH (1:1, v/v) (900 µL) was added and vortexed (2 × 30 s). HCl (1 M, 100 µL, 4 °C) was added and vortexed (2 × 30 s). The samples were centrifuged (3,000 *g*, 3 min, 4 °C) to complete phase separation. 700 µL of the lower organic phase was transferred to a clean tube and dried under $Ar_{(g)}$. The organic residue was reconstituted in ACN/IPA/H_2O (65:30:5, v/v/v) (100 µL) by vortexing (2 × 30 s).

LC-MS/MS. LC-MS/MS analysis was performed on an Acquity CSH C18 column held at 50 °C (2.1 × 100 mm × 1.7 µm particle size; Waters) using an Ultimate 3000 RSLC Binary Pump (400 µL/min; Thermo Scientific). Mobile phase A consisted of 10 mM ammonium acetate in ACN/H_2O (70:30, v/v) containing 250 µL/L acetic acid. Mobile phase B consisted of 10 mM ammonium acetate in IPA/ACN (90:10, v/v) with the same additives. Initially, mobile phase B was held at 2% for 2 min and then increased to 30% over 3 min. Mobile phase B was then further increased to 85% over 14 min and then raised to 99% over 1 min and held for 7 min. The column was then re-equilibrated for 5 min before the next injection. Ten microliters of lipid extract were injected by an Ultimate 3000 RSLC autosampler (Thermo Scientific). The LC system was coupled to a Q Exactive Focus mass spectrometer by a HESI II heated ESI source (Thermo). The MS was operated in polarity switching mode acquiring positive and negative mode MS^1 and MS^2 spectra (Top2) during the same separation. MS acquisition parameters were 17,500 resolving power, 1×10^6 automatic gain control (AGC) target for MS^1 and 1×10^5 AGC target for MS^2 scans, 25 units of sheath gas and 10 units of auxiliary gas, 300 °C HESI II and inlet capillary temperature, 100 ms MS1 and 50 ms MS2 ion accumulation time, 200–1,600 Th MS1 scan range, 1 Th isolation width for fragmentation, stepped HCD collision energy (20, 30, 40 units), 1.0% under fill ratio, and 10 s dynamic exclusion.

Data Analysis. Individual lipid species were identified by searching the discovery LC-MS/MS data against the LipidBlast in-silico lipid spectral library (Kind et al., 2013) with a precursor and product ion tolerance of 0.1 Th. Spectral matches with dot products below 500 were not considered. Matching spectra were manually inspected to ensure proper identification. Lipid quantitation was performed by normalizing the apex MS^1 signal for each identified lipid species to the total identified lipid content.

Yeast LC-MS/MS Lipidomics. Yeast lysates (5 mg protein as quantified by BCA assay, 560 µL) (4 biological replicates of Δ*coq8* yeast and 4 biological replicates of WT yeast; post-diauxic shift cultures) were mixed with $CHCl_3$/MeOH (1:1, v/v) (5 mL) and vortexed (2 × 60 s). HCl (1 M, 560 µL, 4 °C) was added and vortexed (30 s). The samples were centrifuged (1,000 *g*, 5 min, 4 °C) to complete phase separation. 2 mL of the lower organic phase was transferred to a clean tube and dried under $N_{2(g)}$. The organic residue was reconstituted in ACN/IPA/H_2O (65:30:5, v/v/v) (100 µL) by vortexing (2×30 s). Yeast LC-MS/MS and data analysis were conducted essentially as described above for the mouse lipidomics analysis.

Mouse Proteomics and Phosphoproteomics

Sample preparation. Mouse tissues (cerebellum, quadriceps, heart, and kidney) (4 biological replicates of *Coq8a*$^{-/-}$ mice and 4 biological replicates of WT mice, 8-month-old) were homogenized in Proteomics Lysis Buffer [urea (8 M), tris, pH 8 (40 mM), NaCl (30 mM), $CaCl_2$ (1 mM), phosphatase inhibitors (PhosSTOP, Roche), protease inhibitors (cOmplete, Mini, Roche)] at 4 °C (in a cold room) as quickly as possible (< 5 min). Homogenates were lysed on ice using probe sonication. Protein content was evaluated using a BCA assay (Thermo). Proteins were reduced with 5 mM dithiothreitol (DTT) (58 °C, 30 min) and alkylated with 15 mM iodoacetamide (incubation in the dark, ~20 °C, 30 min). Alkylation was quenched by adding additional 5 mM DTT (~20 °C, 15 minutes). Proteins were enzymatically digested in a two-step process. First, proteinase LysC (Wako Chemicals, Richmond, VA) was added to each sample at a ratio of 1:100 (enzyme:protein) and the resulting mixtures were incubated (37 °C, 3 h). Next, samples were diluted to a final concentration of 1.5 M urea (pH 8) with a solution of 50 mM Tris and 5 mM $CaCl_2$. Sequencing-grade trypsin (Promega, Madison, WI) was added to each sample at a ratio of 1:50 (enzyme:protein) and the resulting mixtures were incubated (~20 °C, overnight). The following morning each sample was incubated with an additional aliquot of sequencing-grade trypsin at ratio of 1:100 (enzyme:protein) (~1.5 h). Digests were quenched by bringing the pH ~2 with trifluoroacetic acid and immediately desalted using C18 solid-phase extraction columns (SepPak, Waters).

Desalted material was labeled with TMT 8-plex isobaric labels (Thermo). Prior to quenching the TMT reactions, ~5 µg of material from each TMT channel was combined into a test mix and analyzed by LC-MS/MS to evaluate labeling efficiency and obtain optimal ratios for sample recombination. Following quenching, tagged peptides were combined in equal amounts by mass (~1000 µg per channel for phosphorylation analyses, ~500 µg per channel for protein analyses) and desalted. All experiments had ≥ 98% labeling efficiency, calculated by the number N-terminal labeled peptides divided by the total number of peptide identifications.

Sample fractionation. Labeled peptides were fractionated by strong cation exchange (SCX) using a polysulfoethylaspartamide column (9.4×200 mm; PolyLC) on a Surveyor LC quaternary pump (Thermo). Each dried and mixed TMT sample was re-suspended in buffer A, injected onto the column, and subjected to the following gradient for separation: 100% buffer A from 0–2 min, 0–15% buffer from 2–5 min, and 15–100% buffer B from 5–35 min. Buffer B was held at 100% for 10 minutes and then the column was washed extensively with buffer C and water prior to recalibration. Flow rate was held at 3.0 mL/min throughout the separation. Buffer compositions were as follows: buffer A [5 mM KH_2PO_4, 30% ACN (pH 2.65)], buffer B [5 mM KH_2PO_4, 350 mM KCl, 30% ACN (pH

2.65)] buffer C [50 mM KH_2PO_4, 500 mM KCl (pH 7.5)]. Twelve fractions were collected over the first 50 minute elution period and were immediately frozen, lyophilized, and desalted. A small portion of each, 5%, was extracted and used for protein analysis. The remaining material was retained for phosphopeptide enrichment.

Phosphopeptide Enrichment. Phosphopeptides were enriched using immobilized metal affinity chromatography (IMAC) with magnetic beads (Qiagen). Following equilibration with water, the magnetic beads were incubated with 40 mM EDTA (pH 8.0) for 1 hour, with shaking. Next, the beads were washed four times with water and incubated with 30 mM $FeCl_3$ for 1 hour, with shaking. Beads were then washed four times with 80% acetonitrile/0.15% TFA. Each of the 12 fractions were re-suspended in 80% acetonitrile/0.15% TFA and incubated with the magnetic beads for 45 minutes, with shaking. Bound peptides were washed three times with 80% acetonitrile/0.15% TFA and eluted with 50% acetonitrile, 0.7% NH_4OH. Eluted peptides were immediately acidified with 4% FA, frozen, and lyophilized. Each phospho-peptide fraction was re-suspended in 20 µL 0.2% FA for LC-MS/MS analysis.

LC-MS/MS analysis. All experiments were performed using a NanoAcquity UPLC system (Waters) coupled to an Orbitrap Elite mass spectrometer (Thermo). Reverse-phase columns were made in-house by packing a fused silica capillary (75 µm i.d., 360 µm o.d, with a laser-pulled electrospray tip) with 1.7 µm diameter, 130 Å pore size Bridged Ethylene Hybrid C18 particles (Waters) to a final length of 30 cm. The column was heated to 60 °C for all experiments. Samples were loaded onto the column for 12 minutes in 95:5 buffer A [water, 0.2% formic acid, and 5% DMSO]:buffer B [acetonitrile, 0.2% formic acid, and 5% DMSO] at a flow-rate of 0.30 µL/min. Peptides were eluted using the following gradient: an increase to 7% B over 1 min, followed by a 42 min linear gradient from 7% to 18% B, followed by a 28 min linear gradient from 18% to 27% B, followed by a final 1 min ramp to 75% B which was held for 3 min. The column was equilibrated with 5% buffer B for an additional 25 min. Precursor peptide cations were generated from the eluent through the utilization of a nanoESI source.

Mass spectrometry instrument methods consisted of MS^1 survey scans (1e6 target value; 60,000 resolution; 300 Th – 1500 Th) that were used to guide fifteen subsequent data-dependent MS/MS scans (3 Th isolation window, HCD fragmentation, normalized collision energy of 35; 5e4 target value, 30,000 resolution). Dynamic exclusion duration was set to 30 s, with a maximum exclusion list of 500 and an exclusion width of 0.55 Th below and 2.55 Th above the selected average mass. Maximum injection times were set to 50 ms for all MS^1 scans, 150 ms for MS/MS scans in whole protein analyses, and 200 ms for MS/MS scans in phospho enrichment analyses.

Data Analysis. Data was processed using the in-house software suite COMPASS (Wenger et al., 2011). OMSSA (Geer et al., 2004) (version 2.1.8) searches were performed against a target-decoy database (*UniProt (mouse),* www.uniprot.org, August 7th, 2013). Searches were conducted using a 150 ppm precursor mass tolerance and a 0.015 Da product mass tolerance. A maximum of 3 missed tryptic cleavages were allowed. The fixed modifications specified were carbamidomethylation of cysteine residues, TMT 8-plex on peptide N-termini, and TMT 8-plex on lysine residues. The variable modifications specified were oxidation of methionine and TMT 8-plex on tyrosine residues. Additional variable modifications were specified for phospho-peptide analyses (phosphorylation of threonine, serine, and tyrosine residues). TMT quantification of identified peptides was performed within COMPASS as described previously (Phanstiel et al., 2011). Peptides identified within each of 12 fractions were grouped into proteins according to previously reported rules (Nesvizhskii and Aebersold, 2005) using COMPASS. Phosphopeptide localization was performed using *Phosphinator* software within COMPASS, as described previously (Phanstiel et al., 2011). This program both localized phosphorylation sites and combined quantitative data for phospho-isoforms across all 12 fractions. All phosphosites had to be localized for a given phospho-peptide to be included in subsequent quantitative analysis. Protein quantification was performed by summing all of the reporter ion intensities within each channel for all peptides uniquely mapping back to a given protein. All quantitative data was normalized at the protein level, $\log_2$ transformed and mean normalized. Fold-changes were then calculated by averaging protein-normalized values for each condition and calculating the difference of averages. For each comparison, a *p*-value was calculated using Student's t-test (assuming equal variance) and then correcting for multiple hypotheses (Storey method).

Yeast Proteomics and Phosphoproteomics by LC-MS/MS with Isobaric Tags

Yeast cultures and sample harvests were conducted as described above in the yeast culture methods section (diauxic shift cultures). Yeast proteomics and phosphoproteomics were conducted essentially as described above for the mouse proteomics and phosphoproteomics except 6-plex TMT was used instead of 8-plex TMT. Three sets of 6-plex TMT runs were conducted, each with a biological replicate of the 6 conditions (each 6-plex TMT set contained samples from WT and Δ*coq8* yeast across the three time points).

Yeast Proteomics by Label Free Quantitation LC-MS/MS

Sample preparation. Yeast cultures and sample harvests were conducted as described above in the yeast culture methods section (4 biological replicates of each Coq8p point mutant strain, and 4 biological replicates of WT yeast). Yeast pellets were reconstituted in lysis buffer (8 M urea, 100 mM Tris, pH 8). Proteins were extracted with 90% MeOH and centrifuged (14,000 *g*, 5 min). Pellets were reconstituted in lysis buffer containing 40 mM chloroacetamide and 10 mM tris(2-carboxyethyl)phosphine, and incubated (10 min, ~20 °C). Samples were diluted to a final concentration of 1.5 M urea (pH 8) with 50 mM Tris pH 8. Sequencing-grade trypsin (Promega, Madison, WI) was added to each sample at a ratio of 1:50 (enzyme:protein) and the resulting mixtures were incubated (~12 h, ~20 °C). Digests were quenched by bringing the pH to ~2 with trifluoroacetic acid and immediately desalted using Strata-X polymeric reversed phase solid phase extraction (SPE) columns (Phenomenex). SPE eluants were dried down under vacuum and reconstituted in 0.2% formic acid. Peptide content was determined using a colorimetric assay (Thermo).

LC-MS/MS analysis. All experiments were performed using a NanoAcquity UPLC system (Waters) coupled to an Orbitrap Fusion Tribrid mass spectrometer (Thermo). Reverse-phase columns were made in-house as described above in the section on mouse proteomics. The column was heated to 55 °C using a home-built column heater. Mobile phase solvent A was composed of 0.2% formic acid in water. Mobile phase B was composed of 70% ACN, 0.2% formic acid, and 5% DMSO. For each sample, 2 µg of peptides were loaded on-column and separated over a 120 minute gradient, including time for column re-equilibration. Flow rates were set at 350 µL/min. Precursor scans were performed from 300 to 1,500 m/z at 60K resolution (at 400 m/z) using a 5 x 10^5 AGC target. Precursors selected for tandem MS were isolated at 0.7 Th in the quadrupole and fragments were analyzed using turbo scan in the ion trap. Fragmentation method was based on m/z: precursors above 500 m/z were fragmented by HCD with a normalized collision energy of 27.5, and precursors below 500 m/z were fragmented by CAD with a normalized collision energy of 30. The maximum injection time for MS^2 analysis was 25 ms, with an AGC target of 10^4. Precursors with a charge state of 2–8 were sampled for MS^2. Dynamic exclusion time was set at 15 seconds, with a 25 ppm tolerance around the selected precursor and its isotopes. Monoisotopic precursor selection was turned on. Analyses were performed in top speed mode with 3 second cycles.

Database searching and LFQ analysis. The raw data was processed using MaxQuant (Version 1.5.2.8) (Cox and Mann, 2008). Searches were performed against a target-decoy database of reviewed yeast proteins plus isoforms (UniProt, downloaded January 20, 2013) using the Andromeda search algorithm (Cox et al., 2011). Searches were performed using a precursor search tolerance of 4.5 ppm and a product mass tolerance of 0.35 Da. Specified search parameters included fixed modification for carbamidomethylation of cysteine residues, variable modifications for the oxidation of methionine and protein N-terminal acetylation, and a maximum of 2 missed tryptic cleavages. A 1% peptide spectrum match false discovery rate (FDR) and a 1% protein FDR were applied according to the target-decoy method. Proteins were identified using at least one peptide (razor + unique). Proteins were quantified using MaxLFQ with an LFQ minimum ratio count of 2. LFQ intensities were calculated using the match between runs feature, and MS/MS spectra were not required for LFQ comparisons (Cox et al., 2014).

Recombinant Protein Expression and Purification

Yeast Coq8$^{N\Delta41}$. $Coq8^{N\Delta41}$ plasmid constructs were transformed into RIPL competent *E. coli* cells for protein expression. 8His-MBP-[TEV]-$Coq8^{N\Delta41}$ was overexpressed in *E. coli* by autoinduction (Fox and Blommel, 2009). Cells were isolated by centrifugation, frozen in $N_{2(l)}$, and stored at –80 °C until further use. For protein purification, cells were thawed on ice, resuspended in Lysis Buffer (50 mM HEPES (pH 7.5), 150 mM NaCl, 5% glycerol, 1 mM BME, 0.25 mM PMSF, 1 mg/mL lysozyme, pH 7.5) and incubated (1 h, 4 °C). The cells were lysed by sonication (4 °C, 6 V, 60 s × 4). The lysate was clarified by centrifugation (15,000 *g*, 30 min, 4 °C). The cleared lysate was mixed with cobalt IMAC resin (Talon resin) and incubated (4 °C, 1 h). The resin was pelleted by centrifugation (700 *g*, 5 min, 4 °C) and washed four times with Wash Buffer (50 mM HEPES (pH 7.5), 150 mM NaCl, 5% glycerol, 1 mM BME, 0.25 mM PMSF, 10 mM imidazole, pH 7.5) (10 resin bed volumes). His-tagged protein was eluted with Elution Buffer (50 mM HEPES (pH 7.5), 150 mM NaCl, 5% glycerol, 1 mM BME, 100 mM imidazole, pH 7.5). The eluted protein was concentrated with a MW-cutoff spin filter (50 kDa MWCO) and exchanged into storage buffer (50 mM HEPES (pH 7.5), 150 mM NaCl, 5% glycerol, 1 mM BME, pH 7.5). The concentration of 8His-MBP-[TEV]-$Coq8^{N\Delta41}$ was determined by its absorbance at 280 nm (ε = 109,210 $M^{-1}cm^{-1}$) (MW = 96.2 kDa). The fusion protein was incubated with Δ238TEV protease (1:50, TEV/fusion protein, mass/mass) (1 h, 20 °C). The TEV protease reaction mixture was mixed with cobalt IMAC resin (Talon resin) and incubated (4 °C, 1 h). The unbound $Coq8^{N\Delta41}$ was isolated and concentrated with a MW-cutoff spin filter (30 kDa MWCO) and exchanged into storage buffer. The concentration of $Coq8^{N\Delta41}$ was determined by its absorbance at 280 nm (ε = 41,370 $M^{-1}cm^{-1}$) (MW = 52 kDa). The protein was aliquoted, frozen in $N_{2(l)}$, and stored at –80 °C. Fractions from the protein preparation were analyzed by SDS-PAGE.

Mouse PKA. 8-His-MBP-PKA and PKA (mouse PKA, Prkaca) were isolated as described above for $Coq8^{N\Delta41}$. The concentration of 8His-MBP-[TEV]-PKA was determined by its absorbance at 280 nm (ε = 121,700 $M^{-1}cm^{-1}$) (MW = 84.8 kDa). The concentration of PKA was determined by its absorbance at 280 nm (ε = 53,860 $M^{-1}cm^{-1}$) (MW = 40.5 kDa).

Nucleotide Binding

The general differential scanning fluorimetry (DSF) method (thermal shift assay) has been described previously (Niesen et al., 2007). Mixtures (20 µL total volume) of $Coq8^{N\Delta41}$ (2 µM) or PKA (1 µM) were prepared with SYPRO Orange dye (Life Tech.) (2×), NaCl (150 mM), HEPES (100 mM, pH 7.5), and ligands (e.g. MgATP). Otherwise, the general DSF method, ligand screen, and dissociation constant experiments were conducted as described for $COQ8A^{N\Delta250}$ (Stefely et al., 2015).

In Vitro Kinase Activity

In Vitro Autophosphorylation. Unless otherwise indicated, $Coq8^{N\Delta41}$ (4 µM), MBP-$Coq8^{N\Delta41}$ (4 µM), or PKA (4 µM) was mixed with [γ-^{32}P]ATP (0.25 µCi/µL, 100 µM $[ATP]_{total}$) and $MgCl_2$ (20 mM) in an aqueous buffer (100 mM HEPES, 150 mM NaCl, 0.1 mg/mL BSA, 0.5 mM DTT, pH 7.5) and incubated (30 °C, 60 min, 500 rpm) (final concentrations for reaction components). For the divalent cation screen, $MgCl_2$ and $CaCl_2$ were used at 20 mM. Reactions were quenched with 4×LDS buffer (106 mM TrisHCl, 141 mM Tris base, 2% LDS, 10% glycerol, 0.51 mM EDTA, 0.175 mM Phenol Red, 0.22 mM Coomassie Brilliant Blue G-250, pH 8.5). [γ-^{32}P]ATP was separated from $Coq8^{N\Delta41}$ by SDS-PAGE (10% Bis-Tris gel, MES buffer, 150 V, 1.5 h). The gel was stained with Coomassie Brilliant Blue, dried under vacuum, and imaged by digital photography. A storage phosphor screen was exposed to the gel (~5 days) and then imaged with a Typhoon (GE) to generate the phosphorimages. $COQ8A^{N\Delta250}$ autophosphorylation assays were conducted as described previously (Stefely et al., 2015).

LC-MS/MS of Autophosphorylation Sites. $Coq8^{N\Delta41}$ (WT, A197G, D365N, or A197G,K134H) (20 µM) was mixed with nucleotide (ATP, ADP, or none) (1 mM) in an aqueous buffer (100 mM HEPES, 150 mM NaCl, 20 mM $MgCl_2$, 0.1 mg/mL BSA, 0.5 mM DTT, pH 7.5) and incubated (30 °C, 60 min, 500 rpm). All 12 reactions were conducted in parallel. Reactions were flash frozen in $N_{2(l)}$ after completion. A sample of each autophosphorylation reaction (100 µL) was mixed with lysis buffer (300 µL) (8 M urea, 40 mM Tris (pH = 8.0), 30 mM NaCl, 2 mM $MgCl_2$, 1 mM $CaCl_2$, 1 × phosphatase inhibitor cocktail tablet, and 1 × protease inhibitor tablet). DTT was added (to 2 mM) and incubated (37 °C, 30 min) to reduce disulfide bonds. Alkylation of cysteines was achieved by adding iodoacetimide (to 7 mM) and incubating in the dark (~20 °C, 30 min). The alkylation reaction was quenched by adding DTT (to 7 mM) and incubating (~20 °C, 15 min). Protein was digested with lys-C (37 °C, 4 hours) (1:100, enzyme:protein mass ratio). The sample was diluted to 1.5 M urea with 50 mM Tris (pH = 8.0) and 1 mM $CaCl_2$ solution. Trypsin (1:100, enzyme:protein) was added to further digest the proteins. After overnight incubation at 37 °C, another aliquot of trypsin (1:100, enzyme:protein mass ratio) was added and incubated (1 hour). The digestion was quenched by adding 10% trifluoroacetic acid to bring the pH below 2. The peptides were desalted with Sep-Pak Vac 1cc tC18 cartridges (Waters). Immobilized metal affinity chromatography (IMAC) with magnetic agarose beads (Qiagen) was used to enrich for phosphopeptides (Phanstiel et al., 2011). Both non-phospho and phospho fractions were analyzed by reverse phase nano LC coupled to an Orbitrap Elite (Thermo). All MS raw data were analyzed with COMPASS (Wenger et al., 2011). A precursor mass tolerance of 150 ppm and a product ion mass tolerance of 0.01 Da, and up to 3 missed cleavages with trypsin were applied to searching. Carbamidomethylation of cysteines was set as fixed modification, while oxidation of methionines, phosphorylation with neutral loss on serine and threonine residues, and intact phosphorylation on tyrosine residues were set as variable modifications. Peptides were grouped into parsimonious protein groups by Protein Hoarder at 1% FDR at the unique protein group level.

Protein Kinase Activity. PKA (4 µM) or $Coq8^{N\Delta41}$ (4 µM) and protein substrates [myelin basic protein (Millipore 13-104, 6 µM), none, or a mixture of COQ proteins] were mixed with [γ-^{32}P]ATP (0.3 µCi/µL, 100 µM $[ATP]_{total}$) in an aqueous buffer (100 mM HEPES, 150 mM NaCl, 20 mM $MgCl_2$, 0.1 mg/mL BSA, 0.5 mM DTT, pH 7.5) and incubated (30 °C, 40 min, 500 rpm) (final concentrations for reaction components). The mixture of COQ proteins (COQ3–COQ7 and COQ9) was prepared using a cell-free expression system as described (Floyd et al., 2016, *this issue*). Reactions were quenched with 4×LDS buffer (106 mM TrisHCl, 141 mM Tris base, 2% LDS, 10% glycerol, 0.51 mM EDTA, 0.175 mM Phenol Red, 0.22 mM Coomassie Brilliant Blue G-250, pH 8.5). [γ-^{32}P]ATP was separated from phosphorylated proteins by SDS-PAGE (10% Bis-Tris gel, MES buffer, 150 V, 1.5 h). The gel was stained with Coomassie Brilliant Blue, dried under vacuum, and imaged by digital photography. A storage phosphor screen was exposed to the gel (~5 days) and then imaged with a Typhoon (GE) to generate the phosphorimages.

In Vitro ATPase Activity

ELIPA (Cytoskeleton) assays were carried out according to the manufacturer's instructions with the following modifications. 135 µL of ELIPA mix (75 µL ELIPA Reagent 2, 6 mL of reaction buffer (100 mM HEPES [pH 7.5], 150 mM NaCl, 20 mM $MgCl_2$, 0.5 mM DTT, 0.1 mg/mL Bovine Serum Albumin), 1440 µL ELIPA Reagent 1) was mixed with $Coq8^{N\Delta41}$ (2 µM) (final concentrations). 10 µL of ATP (0–2 mM) (final concentrations) was added to start the reactions (final reaction volume 160 µL), and reactions were incubated (~22 °C). The absorbance at 360 nm was read immediately after adding ATP every minute for 20 minutes. A standard curve was constructed using concentration of inorganic phosphate from 0–25 nmol (0, 0.5, 1, 2.5, 5, 12.5, and 25 nmol). The no enzyme reaction was subtracted from each condition prior to calculation of kinetic constants using SigmaPlot v13.0.

Sub-Cellular Fractionation

Mitochondria were purified from the hearts of 11 C57BL/6 female mice (26-week-old) as previously described (Frezza et al., 2007). Sodium carbonate treatment and subsequent centrifugation were used separate soluble (supernatant) and membrane-anchored (pellet) proteins. First, pure mitochondria were exposed to sodium carbonate (0.1 M, pH 11.5) (30 min, on ice), and then ultracentrifuged (100,000 *g*, 1 h, 4 °C). The soluble and peripheral membrane proteins in the supernatant were TCA-precipitated and then solubilized in sample buffer (10 min, ~20 °C). Ultracentrifuged pellets (integral membrane proteins) were resuspended in sample buffer. Mitochondria were subfractionated using mitochondrial swelling. Mitochondria were resuspended in SEM Buffer (250 mM sucrose, 1 mM EDTA, and 10 mM HEPES-KOH, pH 7.4) and treated with nine volumes of 10 mM HEPES-KOH, pH 7.4 for 15 min on ice, or as a control, kept intact in an equivalent volume of SEM Buffer. Accessible proteins were removed by proteinase K treatment (25 µg/mL) or left untreated as control. PMSF was subsequently added at a concentration of 2 mM to inhibit proteinase K activity. The mitochondria or mitoplasts were then pelleted by centrifugation, washed in SEM Buffer and resuspended in sample buffer. Western blot analyses were conducted as described above in the antibody and WB method section.

Liposome-Protein Co-Floatation

Lipids were extracted from Δ*ubiE E. coli* (~1.2 g wet pellet) with $CHCl_3$/MeOH (1:1, v/v), reduced with excess $NaBH_4$, quenched with AcOH, and re-extracted with $CHCl_3$/MeOH (1:1, v/v). The lipids were dried under $Ar_{(g)}$ to afford 12 mg of dry lipid mass. The lipids were reconstituted in $CHCl_3$/MeOH (1:1, v/v, 1 mL) and stored under $Ar_{(g)}$. To form the *E. coli* extract liposomes, 2.2 mg of *E. coli* lipids were mixed with NBD-PC (17.4 µL, 1 mM), dried under $Ar_{(g)}$, and reconstituted in an aqueous buffer (20 mM Tris, 150 mM NaCl, 1 mM DTT). Liposomes were formed by sonication (22 °C, 30 min, bath sonicator). $Coq8^{N\Delta41}$ (1 µM), $COQ8A^{N\Delta250}$ (1 µM), or $COQ9^{N\Delta79}$ (1 µM) (10 µL protein mixture) was mixed with liposomes (135 µL) and incubated (30 °C, 20 min, 230 rpm). After incubation, the reactions were moved onto ice and mixed with 75% (w/v) sucrose buffer (100 µL) (all sucrose buffers in 20 mM Tris, 150 mM NaCl, 1 mM DTT). Onto this mixture, overlaid 25% sucrose (200 µL) and 0% sucrose (50 µL) in a micro ultracentrifuge tube. Centrifuged (240,000 *g*, 4 °C, 1 h), and isolated 150 µL from the top of the gradient and 150 µL from the bottom of the gradient. Both the top and the bottom fractions were analyzed by SDS-PAGE with sliver staining. Flotation of the liposomes was assessed by tracking NBD-PC fluorescence.

LC-MS/MS of Lipids Co-Purifying with Coq8p

His_8-MBP-$Coq8^{N\Delta41}$ and co-purifying lipids were isolated by cobalt IMAC as described above for protein purification of His_8-MBP-$Coq8^{N\Delta41}$. The elution from the first IMAC was isolated directly without further concentration and snap frozen in $N_{2(l)}$. A sample of His_8-MBP-tagged protein (40 nmol, 310 µL, 129 µM) in "Elution Buffer" (50 mM HEPES, 150 mM NaCl, 5% glycerol, 1 mM BME, 100 mM imidazole, pH 7.5) was mixed with CoQ_6 (internal standard, 0.1 nmol, 10 µL, 10 µM) by vortexing (30 s, 4 °C). $CHCl_3$/MeOH (1:1, v/v) (5 mL) was added and vortexed (2 × 30 s). HCl (1 M, 400 µL) was added and vortexed (30 s). $NaCl_{(aq)}$ (saturated, 1 mL) was added and vortexed (30 s). The samples were centrifuged (1,800 *g*, 4 min, 4 °C) to complete phase separation. The lower organic phase was transferred to a clean tube and dried under $Ar_{(g)}$. The organic residue was reconstituted in ACN/IPA/H_2O (65:30:5, v/v/v) (200 µL) by vortexing (60 s) and transferred to a glass autosampler vial.

Lipids from 10 µL of extract were separated by LC on an Ascentis Express C18 column (150 mm × 2.1 mm × 2.7 µm particle size, Supelco, Bellefonte, PA) using an Accela HPLC pump (Thermo Scientific, San Jose, CA) at a flow-rate of 0.4 mL/min. Mobile phase A was 70/30 acetonitrile/water containing 10 mM ammonium acetate and 0.025% acetic acid and B was 90/10 isopropanol/acetonitrile containing the same additives. At the beginning of the gradient, the flow was maintained at 20% B for 1 min, then ramped to 30% at 4 min, to 50% at 5 min, to 85% at 20 min, to 99% at 21 min, held there until 25 min, returned to 20% B at 25.5 min, and finally the column was re-

equilibrated to 30 min before beginning the next injection sequence. The auto sampler (HTC PAL, Thermo Scientific) vigorously mixed each sample before injection to ensure homogeneity.

The MS conditions were as follows: a Q Exactive mass spectrometer (Thermo Scientific, Build 2.5) was operated in fast polarity switching mode, acquiring both positive and negative mode MS and MS/MS spectra. The mass ranges were 300–1600 Th in positive mode and 200–1600 Th in negative ion mode. Tandem MS acquisition was data dependent, fragmenting the two most abundant precursors from each MS scan with a 10 s exclusion duration. The MS was equipped with a HESI II spray source kept at 350 °C and ± 4 kV. The inlet capillary was kept at 350 °C and sheath and auxiliary gases were set to 35 and 15 units. Resolving power was 17,500 for all scans, AGC target was $1x10^6$ for MS scans and $1x10^5$ for MS/MS scans, the isolation width was 1 Th for MS/MS scans, normalized collision energy was stepped at 20, 30, and 40 units, and maximum injection time was set to 100 ms for MS scans and 50 ms for MS/MS scans. Quantitation was performed by integrating MS^1 elution profiles of lipids using the Xcalibur software suite (Thermo Scientific, Version 3.0).

Protein Co-Expression-Co-Purification

COS cells were transiently transfected with pcDNA3.1 constructs encoding murine COQ8A-FLAG (C-terminal FLAG tag) and COQ3-HA (C-terminal HA tag) or COQ5-HA or COQ9-HA using FuGene 6 according to the manufacturer's instructions. Cells were harvested 24 h after transfection, lysed in a digitonin buffer (50 mM Tris, pH 7.4, 10% glycerol, 100 mM KCl, 0.014% digitonin and 1× Complete Protease Inhibitor Cocktail (Roche)), and a mitochondria-enriched pellet was isolated by centrifugation (10,000 *g,* 10 min, 4 °C). Proteins were extracted from the mitochondria-enriched pellet in a Triton X-100 buffer (10 mM Tris, pH 7.4, 10% glycerol, 100 mM NaCl, 50 mM KCl, 0.2% Triton X-100 and 1× Protease Inhibitors). The protein extract was incubated with anti-FLAG M2 affinity beads (Sigma) (2 h, 4 °C) and eluted with 0.2 M Glycine, pH 2.8.

COQ8A-FLAG Co-Immunoprecipitation-Mass Spectrometry

COQ8A-FLAG Expression in HEK293 Cells. 5 million HEK293 cells were plated into a 15 cm dish with HGDMEM+FBS+P/S (37 °C, 25 mL) and incubated (37 °C, 5% CO_2) until the cultures were ~65–75% confluent (~12–24 h). Cells were transfected by dropwise addition of an OptiMEM+DNA+PEI mixture [900 µL OptiMEM (Thermo) warmed to 37 °C, 20 µg plasmid DNA (pcDNA3.1 COQ8A-FLAG plasmid), 72 µg PEI (72 µL, 1 µg/µL, linear polyethylenimine MW 25,000)] and incubated (37 °C, 5% CO_2, 1 day). After the 1 day of transfection had passed, the media was gently aspirated and replaced with glucose-free DMEM+FBS+P/S with 10 mM galactose (37 °C, 25 mL) and incubated (37 °C, 5% CO_2, 24 h). Immediately prior to cell harvest, the media was aspirated and the cells were gently washed with PBS (~7 mL, ~20 °C). The PBS wash was aspirated, PBS with 1× protease inhibitor cocktail (700 µL, 4 °C) was added, and the cells were harvested by gently scraping and transferring the resuspended cells into a 1.5 mL tube on ice. The cells were isolated by centrifugation (2000 *g*, 1 min, 4 °C). The supernatant was aspirated, and the cell pellets were snap frozen in $N_{2(l)}$ and stored at –80 °C.

Co-Immunoprecipitation. The transfected HEK293 cells were resuspended in Lysis Buffer (200 µL, 4 °C) [20 mM HEPES, pH 7.4, 100 mM NaCl, 10% (w/v) glycerol, 3% (w/v) digitonin (Sigma), 1 mM DTT, protease inhibitors (10 µM benzamidine, 1 µg/mL 1,10-phenanthroline and 0.5 µg/mL each of pepstatin A, chymostatin, antipain, leupeptin, aprotinin; Sigma), phosphatase inhibitors (500 µM imidazole, 250 µM NaF, 300 µM sodium molybdate, 250 µM sodium orthovanadate, 1 mM sodium tartrate; Sigma)]. The cells were vortexed (~15 s) and incubated (10 min, on ice) to lyse the cells. Soluble proteins were isolated by centrifuging (16,000 *g*, 10 min, 4 °C) the lysate to pellet insoluble materials and transferring the supernatant to a clean tube on ice. Anti-FLAG M2 magnetic beads were pre-equilibrated with Final Wash Buffer (20 mM HEPES, pH 7.4, 100 mM NaCl). The soluble protein mixture (equal total masses of protein, 200 µL) was loaded onto the anti-FLAG beads and incubated (60 min, 4 °C, end-over-end agitation). The beads were washed four times with Wash Buffer (170 µL, 4 °C) [20 mM HEPES, pH 7.4, 100 mM NaCl, 0.05% (w/v) digitonin, 10% (w/v) glycerol] and once with Final Wash Buffer (170 µL, 4 °C). Proteins were eluted with Elution Buffer (80 µL, ~21 °C) (20 mM HEPES, pH 7.4, 100 mM NaCl, 0.2 mg/mL 1×FLAG-peptide) (30 min incubation, ~21 °C, 500 rpm shaking) for LC-MS/MS analysis.

Protein digestion. coIP elutions were mixed 1:2 (v/v) with 3 M Urea, 100 mM Tris (pH 8). Protein was reduced with DTT (5 mM, 37 °C, 45 min), alkylated with iodoacetamide (15 mM, in the dark, ~20 °C, 45 min), and alkylation was quenched with an additional 5 mM DTT (~20 °C, 15 min). Protein was enzymatically digested with 0.01 µg/µL of sequencing-grade trypsin (Promega, Madison, WI) (agitation with rocker, ~20 °C, overnight). An additional 0.005 µg/µL of trypsin was added to each sample the next morning and incubated (~20 °C, 1 h). Digests were quenched by bringing the pH below 2 with 10% trifluoroacetic acid and immediately desalted using C18 solid-phase extraction columns (SepPak, Waters, Milford, MA). Peptides were washed with 1 mL of 5% acetonitrile/0.1%

TFA solution on the C18 columns to reduce the abundance of the 1×FLAG peptide from each mixture prior to washing the peptides with 3 mL of 0.1% TFA.

LC-MS/MS analysis. Samples were analyzed on a Dionex UPLC system (Thermo Fisher Scientific, San Jose, CA) coupled to an Orbitrap Elite mass spectrometer (Thermo Fisher Scientific, San Jose, CA). A reverse-phase column was made in-house by packing a fused silica capillary (75 µm i.d., 360 µm o.d., with a laser-pulled electrospray tip) with 3.5 µm diameter, 130 Å pore size Bridged Ethylene Hybrid C18 particles (Waters) to a final length of 30 cm. The column was heated to 55 °C. Samples were re-suspended in 0.2% formic acid and loaded onto the column in 92:8 buffer A [water, 0.2% formic acid, and 5% DMSO] : buffer B [acetonitrile, 0.2% formic acid, and 5% DMSO] at a flow-rate of 0.45 µL/min. Peptides were eluted using the following gradient: an increase to 22% B over 36 min, followed by a 5 min linear gradient from 22% to 28% B, followed by a 3 min linear gradient from 28% to 70% B which was held for 3 minutes. The column was equilibrated with 5% buffer B for an additional 15 min. Precursor peptide cations were generated from the eluent through the utilization of a nanoESI source. To minimize carryover, a 3 run wash sequence was used between samples sets. The first and second washes injected 4.5 µL acetonitrile. The first wash was a short run to trap acetonitrile and the second consisted of a 45 min high organic gradient. A pre-blank wash was run by injecting 4.5 µL 0.2% formic acid using the 60 min gradient described above to allow the identification of carryover proteins. Mass spectrometry instrument methods consisted of MS^1 survey scans ($1x10^6$ target value; 60,000 resolution; 300–1500 Th) that were used to guide fifteen subsequent data-dependent MS/MS scans (2 Th isolation window, HCD fragmentation, normalized collision energy of 30; $5x10^4$ target value, 15,000 resolution). Dynamic exclusion duration was set to 45 s, with a maximum exclusion list of 500 and an exclusion width of ±10 ppm around the selected average mass. Maximum injection times were set to 50 ms for all MS^1 scans and 200 ms for MS/MS scans.

Data analysis. Data was processed using the MaxQuant software suite, version 1.5.2.8 (Cox and Mann, 2008). Searches were performed against a target-decoy database (UniProt (human) database, www.uniprot.org, April 4, 2014, canonical). A maximum of 2 missed tryptic cleavages were allowed. The FTMS MS/MS tolerance was set to 0.015 with the rest of the settings set to the default. Modifications were specified as carbamidomethylation of cysteine residues for fixed and oxidation of methionine for variable. Results grouped into proteins within MaxQuant were filtered to 1% FDR. Proteins were quantified across all samples using MaxLFQ (Cox et al., 2014) with matching between runs within a retention time window of 1 min.

Fluorescence Microscopy

100,000 HEK293 cells were plated onto a poly-D-lysine-coated coverslip in a 6-well dish with HGDMEM+FBS+P/S (37 °C, 2.5 mL) and incubated (37 °C, 5% CO_2) until the culture was ~50% confluent (~24 h). Cells were transfected by dropwise addition of an OptiMEM+DNA+PEI mixture [200 µL OptiMEM (Thermo) warmed to 37 °C, 1 µg pcDNA3.1 COQ8A-FLAG, 0.5 µg plasmid encoding green fluorescent protein with an N-terminal mitochondrial localization sequence (MLS-GFP) (Hanson et al., 2004), and 4.5 µg PEI (4.5 µL, 1 µg/µL, linear polyethylenimine MW 25,000)] and incubated (37 °C, 5% CO_2, 1 day). After 24 hours, the cells were fixed (4% formaldehyde in PBS), permeabilized (0.2% Triton X-100 in PBS), blocked (1% BSA in PBS), and probed with mouse anti-FLAG M2 1° antibody (F1804, Sigma, 1:2000 (v/v) in 0.1% BSA in PBS) and Alexa Fluor 594-conjugated goat anti-mouse 2° antibody (Thermo A-11005, 1:2000 (v/v) in 0.1% BSA in PBS). Cells were stained with Hoechst 33342 dye (1 µg/mL) to label nuclear DNA and placed in mounting medium (1:1, v/v, glycerol/PBS). Microscopy was performed on a Keyence BZ-9000 microscope using 100X oil immersion optics at room temp.

Protein Crystallization and X-Ray Structure

Crystals of selenomethionine-labeled $COQ8A^{N\Delta254}$ R611K were obtained by applying the high throughput screening and optimization platform developed at the Center for Eukaryotic Structural Genomics (Markley et al., 2009). Crystallization screens were set with a TTP Labtech Mosquito robot, and a Tecan Genesis was used for optimization solutions. The best crystals were obtained by hanging drop vapor diffusion using 2 µL of 0.2 mM COQ8A, 2 mM AMPPNP, 4 mM $MgCl_2$ mixed with 2 µL of reservoir solution, 26% sodium acrylate 5100, 20 mM $MgCl_2$, and 100 mM NaHEPES pH 7.5. Crystals were cryopreserved by increasing the sodium acrylate 5100 concentration to 30%. All operations were tracked using SESAME LIMS (Zolnai et al., 2003). Samples were screened for diffraction quality at the LS-CAT and GM/CA beamlines at the Advanced Photon Source. Molecular replacement with the apoprotein structure of wild type COQ8A (ADCK3) 4PED proved difficult, so single-wavelength anomalous diffraction data at 0.9786Ā was collected on a MAR300 CCD detector at GM/CA beamline 23-ID-B. Diffraction data was collected at 100 K, and was reduced with XDS (Kabsch, 2010). The selenium substructure was determined with HySS (Grosse-Kunstleve and Adams, 2003) and phased using Phenix Autosolve (Terwilliger et al., 2009). The model was iteratively improved using ARP/wARP (Langer et al., 2008)-Refmac (Murshudov et al., 1997), Phenix (Afonine et al., 2012)

refinement and Coot (Emsley et al., 2010) with 5% of reflections consistently held in a crossvalidation set. Traditional 2mFo–DFc, mFo–DFc and composite simulated annealing omit maps were calculated throughout the refinement procedure. The final model was continuous from residues 261–644. Electron density for AMPPNP unambiguously places the ADP portion of the ligand, with some ambiguity and potential partial hydrolysis of the terminal imidophosphate group. Electron density for residues 281–298 is relatively poor, probably indicating multiple unresolvable conformations for this portion of the protein. 94% of the residues are in favored backbone conformations and four residues are in disallowed space (Chen et al., 2010).

Identification of Hydrophobic Binding Pockets

The X-ray structures of apo COQ8A (PDB 4PED) and nucleotide-bound COQ8A were subjected to the standard protein preparation procedure implemented in Maestro (Maestro version 9.8, Schrödinger, LLC). The SiteMap module (Halgren, 2007) was used with its default settings to identify the top 5 ranked binding sites on the two structures. Briefly, SiteMap first locates binding sites by grouping site points that are in spatial proximity to the protein and have favorable interaction energies with the protein. For each site identified, it constructs hydrophilic (further divided into donor and acceptor) and hydrophobic maps, and evaluates pockets through their physicochemical properties. The top two ranking pockets found on nucleotide-bound COQ8A are associated with the signature KxGQ domain of COQ8A, and were thus named KxGQ Pocket 1 and KxGQ Pocket 2. The corresponding pockets on apo COQ8A ranked as the first and the fourth, respectively. Overall, due to its different conformation, apo COQ8A encompasses pockets that are less favorable (based on the key evaluation criteria of SiteMap) and less hydrophobic in nature.

Molecular Dynamics (MD) Analysis of COQ8A Structure

PDB structure 4PED was used to model the apo state of COQ8A (residues 261–644) (Stefely et al., 2015). The ADP and ATP bound forms were modeled by replacing AMPPNP in the AMPPNP-COQ8A R611K structure reported here (PDB 5I35) using the homology modeling routine of MODELLER version 9.12 (Fiser et al., 2000). MSE residues in the crystal structure were substituted to MET in our MD simulations. For these MD simulations, we also replaced K611 with R611, as observed in WT COQ8A sequence. Mg^{2+} ions were placed based on the crystal structure of protein kinase A (PDB 1ATP) (Knighton et al., 1991; Zheng et al., 1993). The modeled structures were manually checked for steric clashes before simulation.

MD simulations were performed using GROMACS 5.0.4 (Pronk et al., 2013). AMBER ff99SB-ildn force field (Lindorff-Larsen et al., 2010) was used with parameters for ATP/ADP adopted from previous quantum mechanics calculations (Meagher et al., 2003). The protein was solvated with TIP3P water in a dodecahedron periodic box that was at least 1 nm larger than the protein on all sides. Energy minimization was carried out by coupling steepest descent and conjugate gradient algorithms so that Fmax was less than 50 kcal/mol. Temperature equilibrium was achieved by NVP ensemble in 200 ps at 310 K with a berendsen thermostat. NPT ensemble was done for 200 ps using berendsen thermostat and berendsenbarostat. The positions of the ligand and magnesium ions were restrained in the NVT and NPT equilibration step. The unrestrained MD productions were run for 200 ns using a time step of 2 fs after NPT ensemble for apo/ADP•Mg2+-bound/ATP•Mg2+-bound forms. Root mean square deviation (RMSD) of each simulation was checked to be stable before additional analysis. Torsion angle dynamics were calculated by g_chi programs in the GROMACS package. Kullback–Leibler divergence analysis was performed using mutinf package (McClendon et al., 2009; McClendon et al., 2012). All protein visualization was done using PyMOL.

SUPPLEMENTAL REFERENCES

Afonine, P.V., Grosse-Kunstleve, R.W., Echols, N., Headd, J.J., Moriarty, N.W., Mustyakimov, M., Terwilliger, T.C., Urzhumtsev, A., Zwart, P.H., and Adams, P.D. (2012). Towards automated crystallographic structure refinement with phenix.refine. Acta Crystallogr. D Biol. Crystallogr. *68*, 352–367.

Baudin, A., Ozier-Kalogeropoulos, O., Denouel, A., Lacroute, F., and Cullin, C. (1993). A simple and efficient method for direct gene deletion in Saccharomyces cerevisiae. Nucleic Acids Res. *21*, 3329–3330.

Blommel, P.G., Martin, P.A., Seder, K.D., Wrobel, R.L., and Fox, B.G. (2009). Flexi vector cloning. Methods Mol. Biol. *498*, 55–73.

Chaumont, J., Guyon, N., Valera, A.M., Dugue, G.P., Popa, D., Marcaggi, P., Gautheron, V., Reibel-Foisset, S., Dieudonne, S., Stephan, A.*, et al.* (2013). Clusters of cerebellar Purkinje cells control their afferent climbing fiber discharge. Proc. Natl. Acad. Sci. USA *110*, 16223–16228.

Chen, V.B., Arendall, W.B., Headd, J.J., Keedy, D.A., Immormino, R.M., Kapral, G.J., Murray, L.W., Richardson, J.S., and Richardson, D.C. (2010). MolProbity: all-atom structure validation for macromolecular crystallography. Acta Crystallogr. D Biol. Crystallogr. *66*, 12–21.

Chen, Y.C., Taylor, E.B., Dephoure, N., Heo, J.M., Tonhato, A., Papandreou, I., Nath, N., Denko, N.C., Gygi, S.P., and Rutter, J. (2012). Identification of a protein mediating respiratory supercomplex stability. Cell Metab. *15*, 348–360.

Clark, H.B., Burright, E.N., Yunis, W.S., Larson, S., Wilcox, C., Hartman, B., Matilla, A., Zoghbi, H.Y., and Orr, H.T. (1997). Purkinje cell expression of a mutant allele of SCA1 in transgenic mice leads to disparate effects on motor behaviors, followed by a progressive cerebellar dysfunction and histological alterations. J. Neurosci. *17*, 7385–7395.

Consortium, G.T. (2015). Human genomics. The Genotype-Tissue Expression (GTEx) pilot analysis: multitissue gene regulation in humans. Science *348*, 648–660.

Cox, J., Hein, M.Y., Luber, C.A., Paron, I., Nagaraj, N., and Mann, M. (2014). Accurate proteome-wide label-free quantification by delayed normalization and maximal peptide ratio extraction, termed MaxLFQ. Mol. Cell. Proteomics *13*, 2513–2526.

Cox, J., and Mann, M. (2008). MaxQuant enables high peptide identification rates, individualized p.p.b.-range mass accuracies and proteome-wide protein quantification. Nat. Biotechnol. *26*, 1367–1372.

Cox, J., Neuhauser, N., Michalski, A., Scheltema, R.A., Olsen, J.V., and Mann, M. (2011). Andromeda: a peptide search engine integrated into the MaxQuant environment. J. Proteome Res. *10*, 1794–1805.

Emsley, P., Lohkamp, B., Scott, W.G., and Cowtan, K. (2010). Features and development of Coot. Acta Crystallogr. D Biol. Crystallogr. *66*, 486–501.

Fiser, A., Do, R.K., and Sali, A. (2000). Modeling of loops in protein structures. Protein Sci. *9*, 1753–1773.

Fox, B.G., and Blommel, P.G. (2009). Autoinduction of protein expression. Curr. Protoc. Protein Sci. *Chapter 5*, Unit 5.23.

Frezza, C., Cipolat, S., and Scorrano, L. (2007). Organelle isolation: functional mitochondria from mouse liver, muscle and cultured fibroblasts. Nat. Protoc. *2*, 287–295.

Garcia, S., and Fourcaud-Trocme, N. (2009). OpenElectrophy: An Electrophysiological Data- and Analysis-Sharing Framework. Front. Neuroinform. *3*, 14.

Geer, L.Y., Markey, S.P., Kowalak, J.A., Wagner, L., Xu, M., Maynard, D.M., Yang, X., Shi, W., and Bryant, S.H. (2004). Open mass spectrometry search algorithm. J. Proteome Res. *3*, 958–964.

Gietz, R.D., and Woods, R.A. (2002). Transformation of yeast by lithium acetate/single-stranded carrier DNA/polyethylene glycol method. Methods Enzymol. *350*, 87–96.

Grosse-Kunstleve, R.W., and Adams, P.D. (2003). Substructure search procedures for macromolecular structures. Acta Crystallogr. D Biol. Crystallogr. *59*, 1966–1973.

Halgren, T. (2007). New method for fast and accurate binding-site identification and analysis. Chem. Biol. Drug. Des. *69*, 146–148.

Hebert, A.S., Merrill, A.E., Stefely, J.A., Bailey, D.J., Wenger, C.D., Westphall, M.S., Pagliarini, D.J., and Coon, J.J. (2013). Amine-reactive neutron-encoded labels for highly plexed proteomic quantitation. Mol. Cell. Proteomics *12*, 3360–3369.

Holm, L., Kaariainen, S., Rosenstrom, P., and Schenkel, A. (2008). Searching protein structure databases with DaliLite v.3. Bioinformatics *24*, 2780–2781.

Holt, G.R., Softky, W.R., Koch, C., and Douglas, R.J. (1996). Comparison of discharge variability in vitro and in vivo in cat visual cortex neurons. J. Neurophysiol. *75*, 1806–1814.

Kabsch, W. (2010). Xds. Acta Crystallogr. D Biol. Crystallogr. *66*, 125–132.

Kind, T., Liu, K.H., Lee do, Y., DeFelice, B., Meissen, J.K., and Fiehn, O. (2013). LipidBlast in silico tandem mass spectrometry database for lipid identification. Nat. Methods *10*, 755–758.

Klock, H.E., Koesema, E.J., Knuth, M.W., and Lesley, S.A. (2008). Combining the polymerase incomplete primer extension method for cloning and mutagenesis with microscreening to accelerate structural genomics efforts. Proteins *71*, 982–994.

Knighton, D.R., Zheng, J.H., Ten Eyck, L.F., Ashford, V.A., Xuong, N.H., Taylor, S.S., and Sowadski, J.M. (1991). Crystal structure of the catalytic subunit of cyclic adenosine monophosphate-dependent protein kinase. Science *253*, 407–414.

Langer, G., Cohen, S.X., Lamzin, V.S., and Perrakis, A. (2008). Automated macromolecular model building for X-ray crystallography using ARP/wARP version 7. Nat. Protoc. *3*, 1171–1179.

Lein, E.S., Hawrylycz, M.J., Ao, N., Ayres, M., Bensinger, A., Bernard, A., Boe, A.F., Boguski, M.S., Brockway, K.S., Byrnes, E.J.*, et al.* (2007). Genome-wide atlas of gene expression in the adult mouse brain. Nature *445*, 168–176.

Lindorff-Larsen, K., Piana, S., Palmo, K., Maragakis, P., Klepeis, J.L., Dror, R.O., and Shaw, D.E. (2010). Improved side-chain torsion potentials for the Amber ff99SB protein force field. Proteins *78*, 1950–1958.

Markley, J.L., Aceti, D.J., Bingman, C.A., Fox, B.G., Frederick, R.O., Makino, S., Nichols, K.W., Phillips, G.N., Jr., Primm, J.G., Sahu, S.C.*, et al.* (2009). The Center for Eukaryotic Structural Genomics. J. Struct. Funct. Genomics *10*, 165–179.

McClendon, C.L., Friedland, G., Mobley, D.L., Amirkhani, H., and Jacobson, M.P. (2009). Quantifying Correlations Between Allosteric Sites in Thermodynamic Ensembles. J. Chem. Theory Comput. *5*, 2486–2502.

McClendon, C.L., Hua, L., Barreiro, A., and Jacobson, M.P. (2012). Comparing Conformational Ensembles Using the Kullback-Leibler Divergence Expansion. J. Chem. Theory Comput. *8*, 2115–2126.

Meagher, K.L., Redman, L.T., and Carlson, H.A. (2003). Development of polyphosphate parameters for use with the AMBER force field. J. Comput. Chem. *24*, 1016–1025.

Murshudov, G.N., Vagin, A.A., and Dodson, E.J. (1997). Refinement of macromolecular structures by the maximum-likelihood method. Acta Crystallogr. D Biol. Crystallogr. *53*, 240–255.

Narayana, N., Cox, S., Shaltiel, S., Taylor, S.S., and Xuong, N. (1997). Crystal structure of a polyhistidine-tagged recombinant catalytic subunit of cAMP-dependent protein kinase complexed with the peptide inhibitor PKI(5-24) and adenosine. Biochemistry *36*, 4438–4448.

Nesvizhskii, A.I., and Aebersold, R. (2005). Interpretation of shotgun proteomic data: the protein inference problem. Mol. Cell. Proteomics *4*, 1419–1440.

Niesen, F.H., Berglund, H., and Vedadi, M. (2007). The use of differential scanning fluorimetry to detect ligand interactions that promote protein stability. Nat. Protoc. *2*, 2212–2221.

Phanstiel, D.H., Brumbaugh, J., Wenger, C.D., Tian, S., Probasco, M.D., Bailey, D.J., Swaney, D.L., Tervo, M.A., Bolin, J.M., Ruotti, V.*, et al.* (2011). Proteomic and phosphoproteomic comparison of human ES and iPS cells. Nat. Methods *8*, 821–827.

Pronk, S., Pall, S., Schulz, R., Larsson, P., Bjelkmar, P., Apostolov, R., Shirts, M.R., Smith, J.C., Kasson, P.M., van der Spoel, D.*, et al.* (2013). GROMACS 4.5: a high-throughput and highly parallel open source molecular simulation toolkit. Bioinformatics *29*, 845–854.

Simon, D., Seznec, H., Gansmuller, A., Carelle, N., Weber, P., Metzger, D., Rustin, P., Koenig, M., and Puccio, H. (2004). Friedreich ataxia mouse models with progressive cerebellar and sensory ataxia reveal autophagic neurodegeneration in dorsal root ganglia. J. Neurosci. *24*, 1987–1995.

Stefely, J.A., Reidenbach, A.G., Ulbrich, A., Oruganty, K., Floyd, B.J., Jochem, A., Saunders, J.M., Johnson, I.E., Minogue, C.E., Wrobel, R.L.*, et al.* (2015). Mitochondrial ADCK3 employs an atypical protein kinase-like fold to enable coenzyme Q biosynthesis. Mol. Cell *57*, 83–94.

Terwilliger, T.C., Adams, P.D., Read, R.J., Mccoy, A.J., Moriarty, N.W., Grosse-Kunstleve, R.W., Afonine, P.V., Zwart, P.H., and Hung, L.W. (2009). Decision-making in structure solution using Bayesian estimates of map quality: the PHENIX AutoSol wizard. Acta Crystallogr. D Biol. Crystallogr. *65*, 582–601.

Wenger, C.D., Phanstiel, D.H., Lee, M.V., Bailey, D.J., and Coon, J.J. (2011). COMPASS: a suite of pre- and post-search proteomics software tools for OMSSA. Proteomics *11*, 1064–1074.

Zheng, J., Trafny, E.A., Knighton, D.R., Xuong, N.H., Taylor, S.S., Ten Eyck, L.F., and Sowadski, J.M. (1993). 2.2 A refined crystal structure of the catalytic subunit of cAMP-dependent protein kinase complexed with MnATP and a peptide inhibitor. Acta Crystallogr. D Biol. Crystallogr. *49*, 362–365.

Zolnai, Z., Lee, P.T., Li, J., Chapman, M.R., Newman, C.S., Phillips, G.N., Jr., Rayment, I., Ulrich, E.L., Volkman, B.F., and Markley, J.L. (2003). Project management system for structural and functional proteomics: Sesame. J. Struct. Funct. Genomics *4*, 11–23.